Until now the effect of LPL on HCV was reported by two groups (Thomssen and Bonk, 2002; Andréo et al., 2007). Thomssen and Bonk (2002) treated HCV-positive human sera with LPL derived from *Pseudomonas* spp. (LPL-Ps) and measured HCV RNA titer afterward. They observed destruction of HCV RNA by this treatment, which was blocked by the presence of RNase inhibitors. Because this destruction was dependent on catalytic activity of LPL-Ps, the authors suggested that direct disruption of HCV by this enzyme activity, most likely lysis of virus membranous components, made viral RNA sensitive for RNase present in the reaction mixture. On the other hand, Andréo et al. (2007) reported the effect of bovine LPL on HCV infectivity. They observed that bovine LPL reduced HCV infectivity through its bridging effect between HCV-associated lipoprotein and cells. They described that HCV infectivity was suppressed after association with cellular components followed by subsequent cell entry of HCV, suggesting that LPL-mediated inactivation of HCV required cell interaction.

The former study (Thomssen and Bonk, 2002) focused on the physical change of HCV structure by LPL from *Pseudomonas* spp. that is phylogenetically different from mammals and, thus, it is not clear if the LPL-Ps is physiologically relevant to mammalian LPL. In the latter (Andréo et al., 2007), bovine LPL was shown to reduce HCV infectivity through its bridging effect between HCV-associated lipoprotein and cells. However, the mechanism to reduce HCV infectivity through the interaction with cells in the presence of bovine LPL remains elusive. Thus, so far, the effects of lipolysis of HCV-associated lipoprotein by LPL on HCV infectivity are unclear. Taking account of the studies demonstrating that HCV is associated with lipoproteins, lypolysis activity of LPL and/or HTGL may have direct effects on the property and the infectivity of HCV. Here, we examined the effects of bovine LPL and endogenous human HTGL on the physiological characteristics of HCV-associated lipoproteins and further evaluated the role of lipoproteins on HCV infectivity. We found that LPL and HTGL directly altered the physiological characteristics as well as the infectivity of HCV through their catalytic activities.

Results

HCV infectivity was reduced by bovine LPL treatment

In order to evaluate the association of HCV with lipoproteins and its role in HCV infectivity, we analyzed HCV for sensitivity to LPL. Culture medium of HuH7.5 cells bearing HCV JFH1 genome replication was used as the virus source for this study. The HCV-bearing medium was incubated with bovine LPL (Sigma) and the infectivity was evaluated by adding the LPL-treated medium to naïve HuH7.5 cells. The percentage of HCV-positive cells was dramatically reduced in an LPL dose-dependent manner when HuH7.5 cells were exposed to LPL-treated HCV-bearing medium (Fig. 1a), while treatment with heated LPL, which lost enzymatic activity (Fig. 1b), did not show significant reduction in infectivity (Fig. 1a). Anti-LPL antibody inhibited the reduction in HCV infectivity (Suppl. Fig. 1), indicating that this reduction mainly resulted from LPL itself.

Since enzymatic activity of LPL is shown to inhibit the establishment of HCV infection in cultured cells after virus entry (Andréo et al., 2007), it is possible that our observation results from the same effect of LPL through interaction with cells after virus entry as previously reported. To address the question whether LPL acts on the HCV infectivity through enzymatic effect on the HCV-bearing medium or not, LPL activity was confined to the HCV-bearing medium by using orlistat (Sigma), which inhibits enzymatic activity of LPL (Fig. 1c). When the HCV-bearing medium was treated with orlistat-inactivated LPL, a reduction in infectivity was not observed (Fig. 1d). After treatment of HCV-bearing medium with LPL, we added orlistat to the medium to suppress LPL activity and subsequently inoculated the medium containing inactivated LPL into HuH7.5 cells. Under this condition, LPL-induced reduction in HCV infectivity through interaction with cells, if any, should be suppressed. Therefore, we are able to evaluate the effect of LPL activity on the HCV-bearing medium itself. Significant reduction of HCV infectivity was observed even suppressing LPL activity through interaction with cells (Fig. 1e). These results indicated that LPL could reduce infectivity of HCV which was independent of cellular interaction.

LPL, at the concentration used in this study to reduce HCV infectivity, did not alter the infectivity of Sendai virus (SeV) (Fig. 1f). Therefore, the effects of LPL were likely limited to certain viruses such as HCV due to the nature of LVP. The LPL-induced reduction in HCV infectivity likely results from the lipolytic alteration of a lipoprotein-like structure associating or integrating with HCV. From these results, it is strongly suggested that LPL reduce HCV infectivity through its lipolytic effect on lipoproteins associated with HCV.

Experiments using an MTP inhibitor indicate dependence of HCV release from culture cells on the production of lipoprotein such as VLDL (Huang et al., 2007; Gastaminza et al., 2008). We demonstrated that hydrolysis of HCV-associated lipoprotein by LPL led to a reduction of HCV infectivity. These results imply that HCV could be released from cells as a complex with lipoprotein and that their association could be required for not only their release but also HCV infectivity.

LPL treatment shifted HCV to higher densities

Since the size and buoyant density of VLDL is altered by lipolysis, we speculated that LPL treatment might shift HCV to a higher buoyant density. To examine this possibility, the HCV-bearing medium treated with LPL was ultracentrifuged through iodixanol gradients. Thirty fractions were collected. Core, HCV RNA, and infectivity in each fraction were quantified (Figs. 2a to c). The Core peak shifted from 1.118 toward 1.128 g/ml due to LPL treatment with a dose-dependent manner (Fig. 2a). Fractions with densities from 1.107 to 1.115 g/ml of the undigested HCV sample showed significantly higher infectivity than all other fractions of higher density from the same sample (Fig. 2b). All the LPL-treated fractions showed no infectivity or infectivity lower than that of the untreated fractions (Fig. 2b).

To exclude the possibility that bovine LPL disrupted HCV RNA structure, we quantified HCV RNA in each fraction from untreated and LPL-treated (500 μg/ml) HCV samples. The amount of Core and HCV RNA from all the fractions was not changed by LPL treatment (Figs. 2a and c), indicating that the amount of HCV nucleocapsid estimated by the amount of Core and HCV RNA was not affected by treatment with LPL used in this study. The peak of HCV RNA was observed at a density of the 1.115 g/ml in the untreated control sample, whereas the peak shifted to a density of 1.128 g/ml in the LPL treatment (Fig. 2c). This peak shift in HCV RNA distribution coincided to the shift in peak of Core. Therefore, we suggest that LPL hydrolyzes lipid components from HCV-associated lipoproteins, which results in shifting HCV to higher buoyant densities without substantial changes to the HCV nucleocapsid.

LPL treatment reduced association of HCV with ApoE

To further clarify the effect of LPL on the structure of HCV-associated lipoprotein, we analyzed the association of HCV with ApoB and ApoE. Each fraction of the density gradient centrifugation of LPL-untreated and -treated HCV was subjected to immunoprecipitation using polyclonal antibodies specific for ApoB or ApoE. Subsequently, the immunocomplexes were subjected to RNA extraction followed by quantitative real-time RT-PCR (qRT-PCR). Complexes containing HCV RNAs co-immunoprecipitated with anti-ApoB and anti-ApoE antibodies from LPL-untreated HCV distributed from densities of 1.105 to 1.13, having a peak at 1.115 (Figs. 2d and e), while those from LPL-treated HCV were found in fraction with higher densities (Figs. 2d and e).

LPL affected the association between HCV and ApoB-positive lipoprotein to some extent (Fig. 2d), while it is noticed that the amount

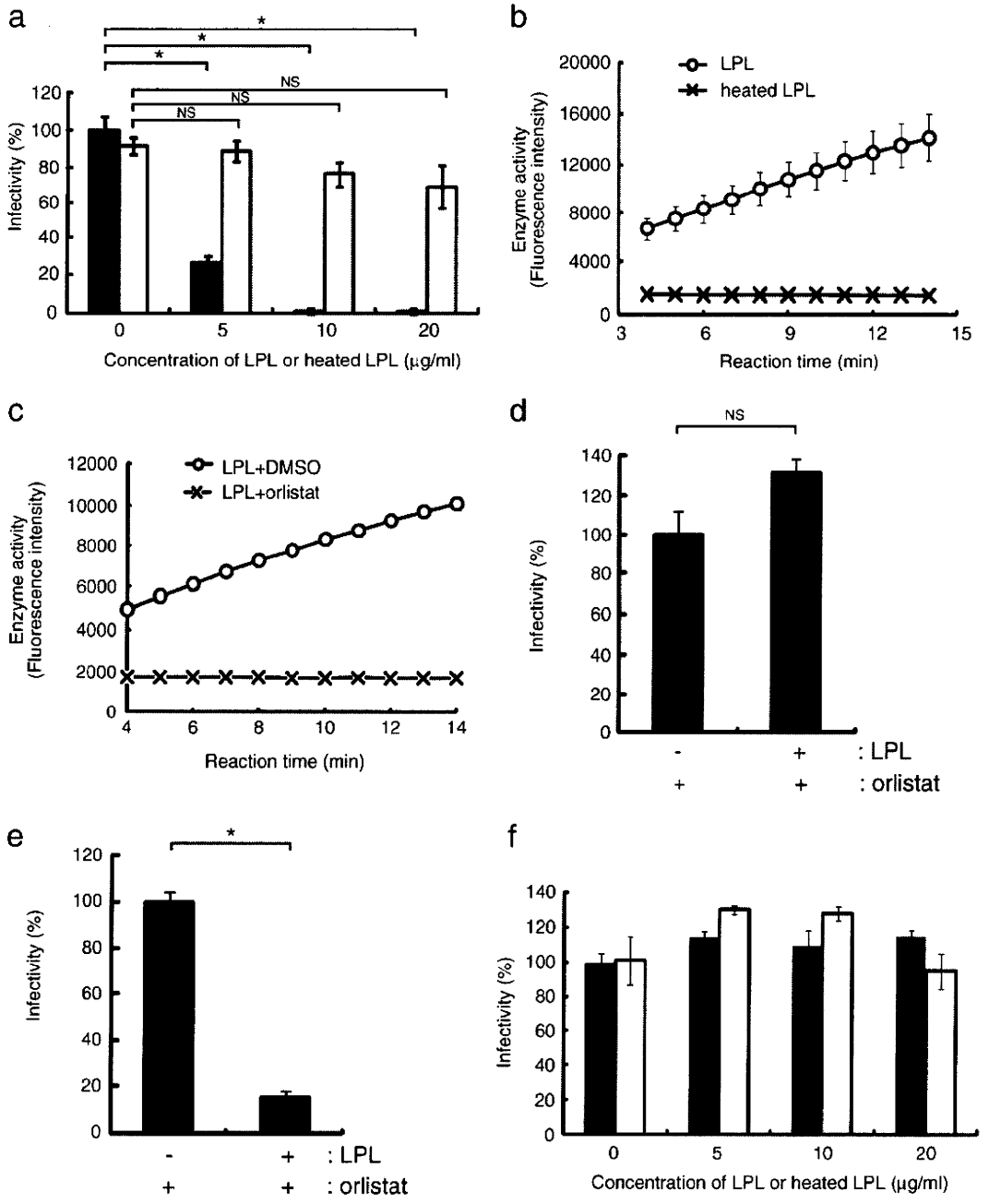

Fig. 1. LPL treatment reduced infectivity of the HCV-bearing medium in a dose-dependent manner. a. The HCV-bearing medium was pretreated with bovine LPL (▮) or heat-inactivated LPL (□) (Fig. 2b) at 37 °C for 1 h before inoculation with HuH7.5 cells. Cells were fixed at 24 h post-inoculation and subjected to immunofluorescence staining. The mean percentage of HCV-positive cells relative to LPL-untreated medium is shown with the standard deviation (n = 3). Statistically significant differences ($p < 0.001$) are indicated by asterisks (Student's *t*-test); NS (not significant, $p > 0.01$). b. Activities of LPL and inactivated LPL by heating at 100 °C for 5 min were determined. The mean value and standard deviation are shown (n = 3). c. Activities of LPL on incubation with orlistat were determined. LPL (10 μg/ml) and orlistat (25 μg/ml) were mixed and subjected to determine lipase activity. Orlistat completely inhibited LPL activity. The mean value and standard deviation are shown (n = 3). d. The HCV-bearing medium was pretreated with LPL (10 μg/ml) and orlistat (25 μg/ml) at 37 °C for 1 h before inoculation. Cells were subjected to immunofluorescence staining at 24 h post-inoculation. The mean percentage of HCV-positive cells relative to LPL-untreated medium is shown with the standard deviation (n = 3). There was no statistically significant difference observed (Student's *t*-test): NS $p > 0.01$. e. Orlistat (25 μg/ml) was added just before HuH7.5 cells were inoculated with the HCV-bearing medium pretreated with LPL (10 μg/ml). Cells were subjected to immunofluorescence staining at 24 h post-inoculation. The mean percentage of HCV-positive cells relative to LPL-untreated medium is shown with the standard deviation (n = 3). Statistically significant differences are indicated by asterisks (Student's *t*-test): *$p < 0.001$. f. SeV, whose genome contains the gene coding Green Fluorescent Protein (GFP), was pretreated with bovine LPL (▮) or heat-inactivated LPL (□) (Fig. 2b) at 37 °C for 1 h before inoculation with HeLa cells. Expression of GFP in infected cells was observed under microscope at 24 h post-inoculation. The mean percentage of SeV-positive cells relative to LPL-untreated medium is shown with the standard deviation (n = 3). LPL did not significantly affect the infectivity of SeV ($p > 0.01$).

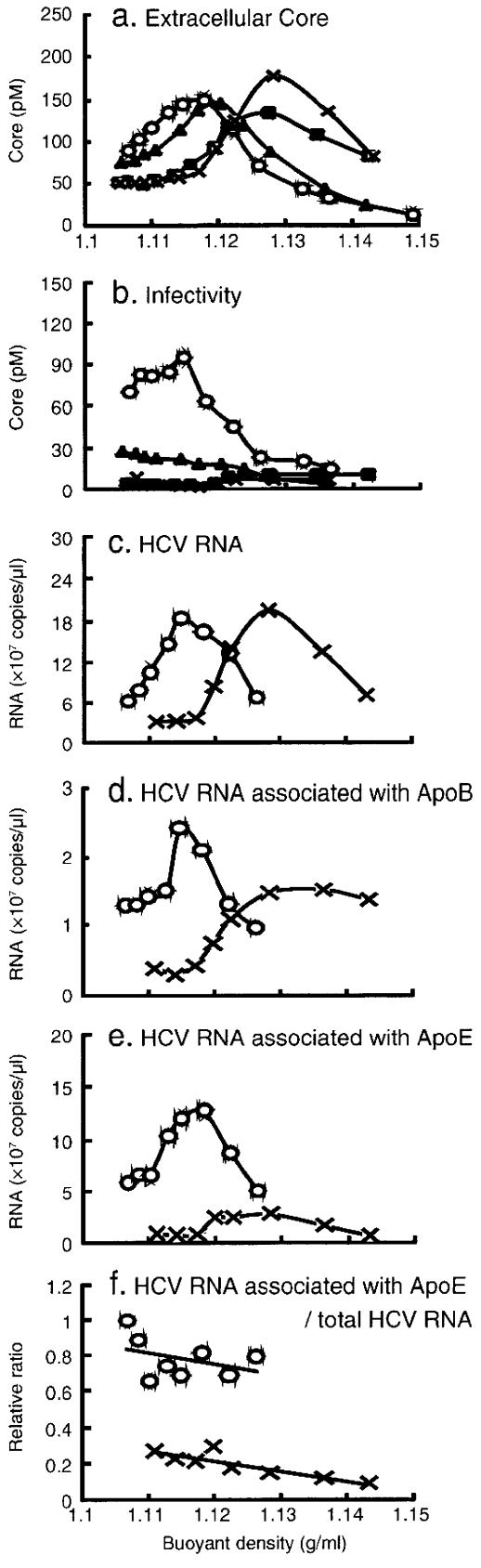

of HCV RNA in the complex associating with ApoE from LPL-treated sample was remarkably reduced (Fig. 2e). Thus, it is indicated that HCV is associated with both ApoB and ApoE but that the association with ApoE is more closely related to HCV infectivity than that with ApoB.

The ratio of HCV RNA in the complex associating with ApoE to the total HCV RNA was dramatically lower in LPL-treated samples than in PBS-treated samples (Fig. 2f). HCV with the same buoyant density showed a different ratio of the association with ApoE between LPL-treated and -untreated samples (Fig. 2f). It is indicated that HCV with the same buoyant density might have heterogeneous characteristics, especially in the association with ApoE. Though LPL affects the buoyant density of HCV, buoyant density may not become a direct indicator of HCV infectivity.

LPL and HTGL reduced HCV infectivity

Generally, two successive lipolytic steps, sequentially catalyzed by LPL and HTGL, convert VLDL through IDL to LDL (Braun and Severson, 1992; Connelly, 1999; Mead et al., 2002; S.-Fojo et al., 2004). Hepatocytes produce HTGL but not LPL (Braun and Severson, 1992; Connelly, 1999). If HuH7.5 cells produce HTGL into culture medium, addition of LPL to the HCV-bearing medium from HuH7.5 cells would lead to two successive lipolytic actions by exogenous LPL and endogeneous HTGL. To analyze this possibility, we examined HTGL expression in HuH7.5 cells. Expression of LPL mRNA in hepatocyte-derived cell lines, HuH7.5 and HepG2, was lower compared to that in the 293T cell line derived from kidney (Fig. 3a). We observed higher expression of HTGL mRNA in HuH7.5 and HepG than in 293T (Fig. 3a). HTGL activity was detected in medium from HuH7.5 cells, which was higher than that in medium from 293T cells (Fig. 3b) and showed good agreement to the level of mRNA (Fig. 3a), though HTGL activity was not detected in medium from HepG2 cells.

Then, to evaluate the role of HTGL on LPL-induced reduction of HCV infectivity, the HCV-bearing medium was incubated with LPL in the presence of a neutralizing antibody against HTGL and infectivity was measured. Since LPL activity itself was not affected by the anti-HTGL antibody treatment (data not shown), we expected that HCV-associated lipoprotein should be protected against HTGL in the presence of the anti-HTGL antibody. In fact, LPL-induced reduction in HCV infectivity was partly suppressed by the presence of the anti-HTGL antibody (Fig. 3c). The infectivity was not fully restored after treatment with the anti-HTGL antibody from the LPL-induced suppressive status, which indicates that HTGL plays a partial role in the LPL effect but that LPL also plays a role. This result implied that two lipases could reduce HCV infectivity through changing the lipoprotein-like structure and that, conversely, infectivity of HCV was regulated by the lipoprotein-like structure that associated with HCV.

HTGL reduced HCV infectivity through its catalytic activity, irrespective of LPL activity

To confirm the reductive effect of HTGL on HCV infectivity, the endogenous expression of HTGL was suppressed by siRNA specific to

Fig. 2. Shift of buoyant density of HCV as well as detachment of ApoE by LPL treatment. The HCV-bearing medium treated with PBS or LPL was subjected to centrifugation in an iodixanol gradient. After ultracentrifugation, aliquots of 30 consecutive fractions were collected and analyzed for (a) Core, (b) infectivity, (c) HCV RNA, and HCV RNA in (d) ApoB-associated and (e) ApoE-associated complexes. For a and b, PBS (○), 5 (▲), 50 (■), and 500 (×) μg/ml of LPL-treated samples, and for c–f, PBS (○) and 500 (×) μg/ml of LPL-treated samples were subjected. a. Core in each fraction was measured by ELISA (Ortho Clinical Diagnostics). b. HuH7.5 cells were inoculated with aliquots of each fraction for 2 h. Core ELISA of the culture medium was performed at 24 h post-inoculation. c. RNA was extracted from each fraction and subjected to cDNA synthesis followed by quantitative PCR. d. Measurement of HCV RNA in the complexes associated with ApoB. e. Measurement of HCV RNA in the complexes associated with ApoE. f. Ratio of HCV RNA in the complexes associated with ApoE versus the total HCV RNA in each fraction. The values were obtained by dividing the amounts of RNA of Fig. 3e by those of Fig. 3c.

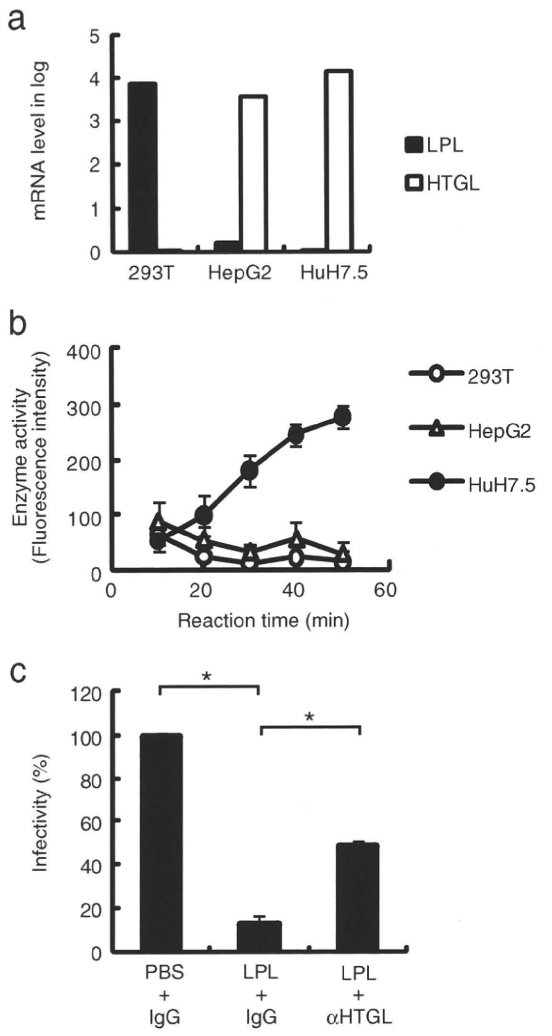

Fig. 3. Treatment of the HCV-bearing medium with exogenous LPL led to subsequent digestion by endogenously produced HTGL, resulting in loss of HCV infectivity. a. Expression of LPL and HTGL in HuH7.5, HepG2 and 293T cells. The mean of LPL mRNA expression level in 293T cells relative to the level in HuH7.5 cells is shown with standard deviation (n=3) and vice versa for HTGL (n=3). b. Validation of HTGL activity. The culture medium from HuH7.5, HepG2 and 293T cells was concentrated to 20 times using centricon YM-30 (Millipore), and was analyzed for HTGL activity. The mean and standard deviation are shown (n=3). c. The HCV-bearing medium was incubated with anti-HTGL antibody before LPL treatment. HuH7.5 cells were inoculated with the medium and then subjected to immunofluorescence staining at 24 h post-inoculation. The mean percentage of HCV-positive cells relative to medium incubated with PBS and IgG is shown with the standard deviation (n=3). Statistically significant differences are indicated by asterisks (Student's *t*-test): $^{*}p<0.001$.

HTGL (Fig. 4a). The level of HTGL mRNA in cells transfected with siRNA targeting HTGL was lower than one 6th of the control cells transfected with non-target siRNA (Fig. 4a). The activity of secreted HTGL was slightly lower in HTGL knockdown cells than the control (Fir. 4b). It may be because HTGL is so stable at protein level that its activity remains 48 h after transfection of siRNA. The presence of infectious HCV in the cells as well as the amounts of Core secreted into the culture medium was not significantly different between HTGL knockdown cells and the control (Fig. 4a). ApoB and ApoE were secreted at the same level from HTGL knockdown cells and the control cells (Fig. 4c). These results indicate that HTGL knockdown did not affect the production of either HCV or lipoproteins. Interestingly, the infectivity of the culture medium was about 2 folds higher than that in culture medium from control cells (Fig. 4a). The HCV-bearing medium from HTGL knockdown cells was ultracentrifuged through iodixanol gradients. We collected 80 fractions from the gradients and analyzed for Core. The Core peak was shifted to a lower buoyant density in the medium from HTGL knockdown cells compared to the control (Fig. 4d). Thus, HTGL could hydrolyze HCV-associated lipoproteins in the medium derived from HuH7.5 cells irrespective of LPL, leading to a reduction of infectivity.

Discussion

Our results indicate that bovine LPL reduced HCV infectivity through its catalytic activity. Since the same doses of LPL did not impair the infectivity of SeV (Fig. 1f), it is likely that HCV-associated lipoprotein is targeted by the LPL and that the lipoprotein associating with HCV plays a pivotal role in HCV infectivity. Previously, it was shown that LPL-Ps disrupted HCV (Thomssen and Bonk, 2002) and that bovine LPL suppressed HCV infectivity through uncertain mechanisms within cells after bridging HCV with cells by bovine LPL (Andréo et al., 2007). We detected Core and HCV RNA from the LPL-treated HCV-bearing medium almost at the same level as the untreated medium (Figs. 2a and c). Thus, bovine LPL at the concentration used in this study did not destroy the HCV structure as reported by LPL-Ps (Thomssen and Bonk, 2002). LPL seems to have at least two distinct functions to reduce HCV infectivity; one is through its de-lipidation activity observed here and another is its suppressive activity observed after being associated with cells (Andréo et al., 2007). We used an LPL inhibitor, orlistat, to delineate these two suppressive functions of LPL on HCV. After incubation of the HCV-bearing medium with LPL at a concentration of 10 μg/ml, orlistat was added so that catalytic activity of LPL could be suppressed upon contact of HCV with cells. HCV infectivity was significantly reduced even under this condition (Fig. 1e). This result indicates that de-lipidation by LPL is a major cause of HCV inactivation. However, it is worth mentioning that the residual infectivity was higher than that observed in the conditions of infection assay conducted without orlistat (Fig. 1e, compare the lane with the same dose (10 μg/ml) of LPL in Fig. 1a), which indicates the presence of another inactivating mechanism suggested by Andréo et al. (2007) though the contribution is not as high.

The experiments using neutralizing antibody against HTGL (Fig. 3c) indicated that both LPL and HTGL have some roles in LPL-induced reduction in HCV infectivity. Knockdown of HTGL resulted in HCV with higher infectivity and a lower density in the medium (Figs. 4a and d). HTGL is the predominant enzyme in the lipolysis of IDL, but also hydrolyzes TG in all lipoproteins to some extent (Connelly, 1999). Thus, it is suggested that endogenous HTGL has lipolytic activity on HCV-associated lipoprotein irrespective to LPL functions. Taking account of the effect of LPL and HTGL on HCV infectivity, their expression is disadvantageous for HCV. There were not much differences in expressions of LPL and HTGL between HuH7.5 cells and HepG2 cells (Fig. 3a), suggesting that expression of lipases does not explain HuH7.5 as an excellent cell line for HCV.

Our study shows that LPL and/or HTGL change(s) the nature of HCV-associated lipoproteins, leading to reduced HCV infectivity. This indicates that the association of HCV with certain lipoprotein-like VLDL is important for HCV infectivity. Recently, ApoE was shown to be important for HCV infectivity as a ligand of the HCV receptor (Owen et al., 2009). It is conceivable that the reduction of ApoE in accordance to lipolysis of HCV associating lipoproteins is a direct cause of the reduction of HCV infectivity.

We used bovine LPL at 2–20 μg/ml to reduce HCV infectivity (Fig. 1a). It is expected that the same doses of human LPL could reduce HCV infectivity. However, heparin-treated human plasma contains around 100 ng/ml of LPL; most of LPL is bound to heparan sulfate proteoglycan (HSPG) at the cell surface and

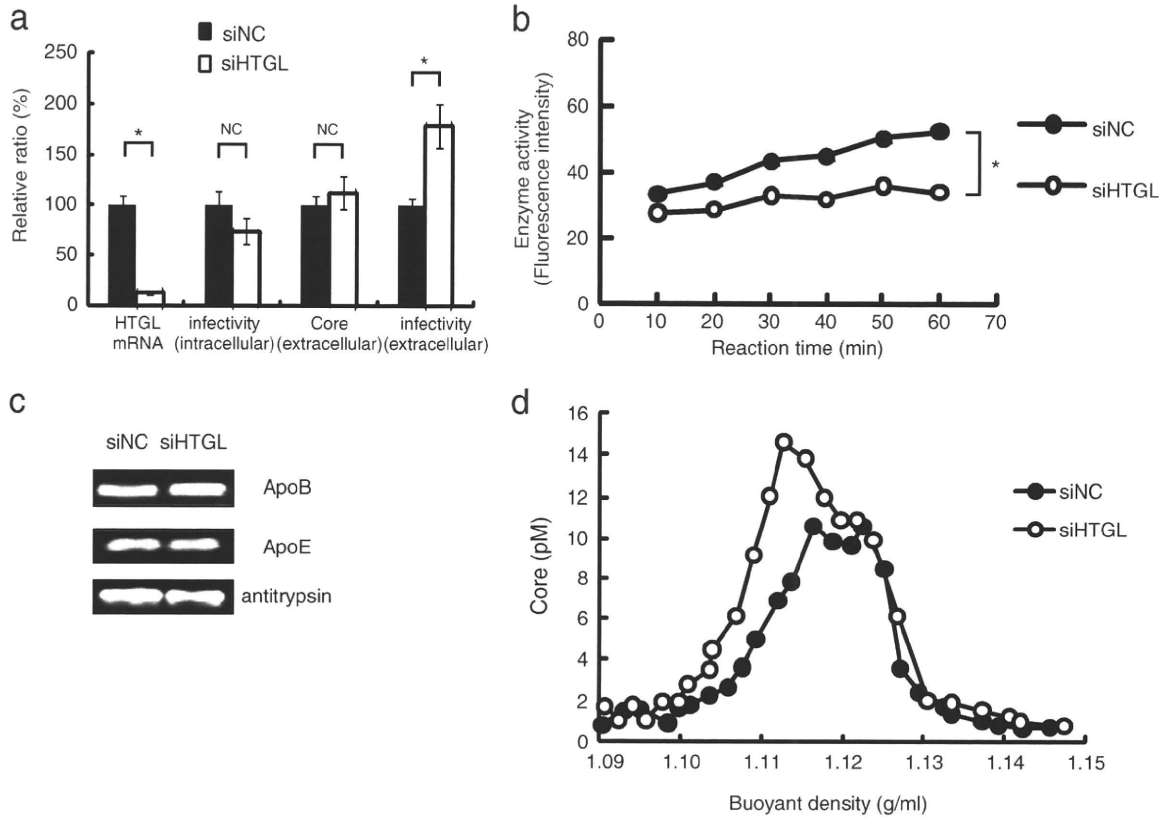

Fig. 4. HCV with higher infectivity and a lower buoyant density in the medium from HTGL knockdown cells. a. HTGL mRNA, infectivity of HCV within cells, extracellular Core and infectivity of HCV in the medium are shown. The mean percentages relative to control cells are shown with the standard deviation (mRNA, Core; n = 3, infectivity; n = 5). Statistically significant differences in HTGL mRNA level and extracellular infectivity are indicated by asterisks (Student's *t*-test): $^*p<0.001$. There was no statistically significant difference in intracellular infectivity and extracellular core (Student's *t*-test): NS $p>0.01$. b. Activities of HTGL were determined. After secretion, most of the HTGL is bound to heparan sulfate proteoglycans (HSPG) at the cell surface (Connelly, 1999; S.-Fojo et al., 2004). Both HTGLs bound and unbound to HSPG are expected to act on lipoproteins in the medium. Thus, in order to evaluate activities of HTGL acting on lipoproteins in the medium, heparin (10 U/ml) was added to the medium to release HTGL bound to HSPG at 24 h post-transfection of siRNA. The medium was harvested at 48 h post-transfection, passed through 0.45 μm filter (Iwaki) to eliminate cell debris and used for the assay. Statistically significant difference in HTGL activity at 60 min is indicated by asterisks (Student's *t*-test): $^*p<0.001$. c. Detection of apolipoproteins (ApoB and ApoE) and α-1 antitrypsin as standard secreted in culture medium from HTGL knockdown cells and control cells. d. Buoyant density of HCV produced from HTGL knockdown cells. The HCV-bearing medium from HTGL knockdown cells was subjected to centrifugation in an iodixanol gradient. After ultracentrifugation, aliquots of 80 consecutive fractions were collected and analyzed for Core by ELISA. The data are presented from 25 fractions around Core peak from a single representative experiment of three experiments. There was a significant difference in the buoyant density of the Core peak between HTGL knockdown cells and the control (Student's *t*-test, $p<0.001$).

heparin leads to a release of LPL bound to HSPG (Kern et al., 1990). Therefore, it is conceivable that HCV infectivity could be reduced through activities of LPL in the circulation at a lesser efficiency than observed in this work. Here, we demonstrated that the hydrolyzing activity of HTGL as well as LPL affects HCV infectivity. Considering this lipase-induced reduction in HCV infectivity in the circulation, it is important for virus to infect the proximal hepatocytes before entering circulation. In other words, the activities of LPL and/or HTGL may be one host mechanism to resist invasion and spread of HCV.

Materials and methods

Cell culture

HuH7.5, HeLa, 293T and HepG2 cells were maintained in DMEM supplemented with 10% FBS, 100 U/ml penicillin and 100 μg/ml streptomycin.

Virus source

HuH7.5 cells were transfected with HCV 2a strain, JFH1 RNA genome and maintained in DMEM supplemented with 10% FBS, 100 U/ml penicillin and 100 μg/ml streptomycin. Three days before harvest, medium was replaced with Opti-Pro (Invitrogen) supplemented with 0.1% BSA. Culture medium was filtered with 0.45 μm filter (Iwaki) and used as virus source (the HCV-bearing medium).

HCV infectivity

To determine HCV infectivity in the medium, HuH7.5 cells were inoculated with the HCV-bearing medium (MOI of 0.5) at 37 °C for 2 h. Cells were washed with PBS and incubated in DMEM supplemented with 10% FBS, 100 U/ml penicillin and 100 μg/ml streptomycin. Cells were fixed at 24 h post-inoculation and subjected to immunofluorescence staining using serum from a HCV-positive individual to detect HCV-infected cells. Three to five fields under microscope were randomly selected. Cells in a field were counted and the percentage of HCV-positive cells to total cells (around 500–1000) was calculated.

To determine HCV infectivity within cells, cells were collected by trypsinization. After washing with PBS, cells were incubated with water and passed through a 27-gauge needle (Terumo) at ten times. After centrifugation, supernatant was passed through a 0.45 μm filter (Iwaki) and inoculated to HuH7.5 cells. Immunofluorescence staining was performed as mentioned above.

Lipase activity

Total lipase test (Progen) and hepatic lipase select test (Progen) were used to examine LPL activity and HTGL activity, respectively, according to the manufacturer's protocol.

Iodixanol density gradients

The HCV-bearing medium was concentrated around 50 times using amicon ultra-15 100k (Millipore) and treated with PBS or 5, 50, or 500 μg/ml of LPL at 37 °C for 1 h. The samples were applied to the top of a linear gradient formed from 17–37% iodixanol-containing PBS and spun at 36,000 rpm for 18 h at 4 °C using a SRP 41 Hitachi Ultracentrifuge rotor. Aliquots of 30 consecutive fractions were collected and used for analyses of Core, infectivity, HCV RNA, and immunoprecipitation with anti-ApoB or anti-ApoE antibodies.

For analysis of the HCV-bearing medium from HTGL knockdown cells, the concentrated samples were applied to the top of a gradient from 14–54% iodixanol-containing PBS and spun at 34,000 rpm for 20 h at 4 °C. A total of 80 consecutive fractions were collected and used for analyses of Core.

Quantification of HCV RNA

RNA was extracted from fractions of the iodixanol gradient using an RNeasy mini kit (Qiagen). Complementary DNA was prepared by incubating RNA with SuperScript III (Invitrogen) and 737R primer, a reverse RNA primer of HCV genome (Sugiyama et al., 2009). Quantitative PCR analysis was performed by 7500 Fast Real Time PCR System (Applied Biosystems). Taqman probe and primers were as follows: probe 733FB (Sugiyama et al., 2009), forward 5′-CCCTCCCGGGAGAGCCATAGTG-3′, reverse 5′-GTCTCGCGGGGGCACGCCCAAAT-3′. The copy number of HCV was determined by the standard-curve method with serial dilutions of the synthesized full-length HCV RNA.

Immunoprecipitation

Fractions from iodixanol gradient were incubated with anti-ApoB antibody (Biodesign International) or anti-ApoE antibody (Chemicon International) for 2 h at room temperature. Protein G sepharose (GE) was added and the immunocomplex was collected by centrifugation. The pellets were used for RNA extraction.

Expression of LPL and HTGL

RNA was extracted from cells using RNeasy mini kit (Qiagen). Complementary DNA was prepared by incubating RNA with Super-Script III (Invitrogen) and oligo(dT) as an universal primer. Quantitative PCR analysis was performed with primers specific for LPL (Lindegaard et al., 2005), for HTGL (Sirvent et al., 2004), and for GAPDH (Suzuki et al., 2008). The LPL and HTGL mRNA expression level was calibrated with the level of GAPDH mRNA expression.

Neutralization of HTGL

The HCV-bearing medium was incubated with IgG rabbit (Santa Cruz) or anti-HTGL antibody (sc-21007, Santa Cruz) at 4 °C overnight, followed by PBS or LPL treatment at 37 °C for 1 h. HuH7.5 cells were inoculated with the medium at 37 °C for 2 h and subjected to immunofluorescence staining as explained above.

Knockdown of HTGL

siRNA (siGENOME SMART pool M-008743-00-0005, Thermo) at a final concentration of 40 nM was transfected with HuH7.5 cells using siLentFect reagent (Bio-Rad). The HCV-bearing medium (MOI = 0.5) was inoculated with cells at 4 h post-transfection. Then, fresh medium was replaced 2 h later. At 24 h post-transfection, medium was replaced with Opti-pro (Invitrogen) supplemented with 0.1% BSA. At 48 h post-transfection, culture medium and cells were used for analyses of RNA, infectivity, Western blotting and buoyant density.

Western blotting

Western blotting was performed using anti-ApoB antibody (Biodesign International), anti-ApoE antibody (Innogenetics) and anti-α-1 antitrypsin antibody (Biodesign). Detection was carried out using ECL plus reagent (GE).

Supplementary materials related to this article can be found online at doi:10.1016/j.virol.2010.08.011.

Acknowledgments

We are grateful to Drs. T. Wakita and C. Rice for their kind gifts of JFH1 and HuH7.5 cells, respectively. We thank H. Kato, R. Shiina, E. Sugawara, R. Tobita, and H. Yamamoto (Chiba Institute of Technology) for their technical assistance. This study was supported by Grants-in-Aid for Scientific Research from the Ministry of Health, Labor, and Welfare of Japan and from the Ministry of Education, Culture, Sports, Science, and Technology.

References

André, P., K.-Pradel, F., Deforges, S., Perret, M., Berland, J.L., Sodoyer, M., Pol, S., Bréchot, C., P.-Baccalà, G., Lotteau, V., 2002. Characterization of low- and very-low-density hepatitis C virus RNA-containing particles. J. Virol. 76, 6919–6928.

Andréo, U., Maillard, P., Kalinina, O., Walic, M., Meurs, E., Martinot, M., Marcellin, P., Budkowska, A., 2007. Lipoprotein lipase mediates hepatitis C virus (HCV) cell entry and inhibit HCV infection. Cell. Microbiol. 9, 2445–2456.

Braun, J.E.A., Severson, D.L., 1992. Regulation of the synthesis, processing and translocation of lipoprotein lipase. Biochem. J. 287, 337–347.

Chang, K.-S., Jiang, J., Cai, Z., Luo, G., 2007. Human apolipoprotien E is required for infectivity and production of hepatitis C virus in cell culture. J. Virol. 81, 13783–13793.

Connelly, P.W., 1999. The role of hepatic lipase in lipoprotein metabolism. Clin. Chim. Acta 286, 243–255.

Gastaminza, P., Cheng, G., Wieland, S., Zhong, J., Liao, W., Chisari, F.V., 2008. Cellular determinants of hepatitis C virus assembly, maturation, degradation, and secretion. J. Viol. 82. 2120–2129.

Huang, H., Son, F., Owen, D.M., Li, W., Chen, Y., Gale Jr., M., Ye, J., 2007. Hepatits C virus production by human hepatocytes dependent on assembly and secretion of very low-density lipoprotein. Proc. Natl Acad. Sci. 104, 5848–5853.

Icard, V., Diaz, O., Scholtes, C., P.-Cocon, L., Ramière, C., Bartenschlager, R., Penin, F., Lotteau, V., André, P., 2009. Secretion of hepatitis C virus envelope glycoproteins depends on assembly of apolipoprotein B positive lipoproteins. PLoS ONE 4, e4233.

Jiang, J., Luo, G., 2009. Apolipoprotein E but not B is required for the formation of infectious hepatitis C virus particles. J. Virol. 83, 12680–12691.

Kern, P.A., Martin, R.A., Carty, J., Goldberg, I.J., Ong, J.M., 1990. Identification of lipoprotein lipase immunoreactive protein in pre- and posthepain plasma from normal subjects and patients with type I hyperlipoproteinemia. J. Lipid Res. 31, 17–26.

Lindegaard, M.L.S., Olivecrona, G., Christoffersen, C., Kratky, D., Hannibal, J., Petersen, B.L., Zechner, R., Damm, P., Nielsen, L.B., 2005. Endothelial and lipoprotein lipases in human and mouse placenta. J. Lipid Res. 46, 2339–2346.

Mead, J.L., Irvine, S.A., Ramji, D.P., 2002. Lipoprotein lipase: structure, function, regulation, and role in disease. J. Mol. Med. 80, 753–769.

Olofsson, S.-O., Borèn, J., 2005. Apolipoprotein B: a clinically important apolipoprotein which assembles atherogenic lipoproteins and promotes the development of atherosclerosis. J. Intern. Med. 258, 395–410.

Owen, D.M., Huang, H., Ye, J., Gale Jr., M., 2009. Apolipoprotein E on hepatitis C virion facilitates infection through interaction with low-density lipoprotein receptor. Virology 394, 99–108.

S.-Fojo, S., G.-Navarro, H., Freeman, L., Wagner, E., Nong, Z., 2004. Hepatic lipase, lipoprotein metabolism, and atherogenesis. Arterioscler. Thromb. Vasc. Biol. 24, 1750–1754.

Sirvent, A., Verhoeven, A.J.M., Jansen, H., Kosykh, V., Darteil, R.J., Hum, D.W., Fruchart, J.-C., Staels, B., 2004. Farnesoid X receptor represses hepatic lipase gene expression. J. Lipid Res. 45, 2110–2115.

Sugiyama, K., Suzuki, K., Nakazawa, T., Funami, K., Hishiki, T., Ogawa, K., Saito, S., Shimotohno, K.W., Suzuki, T., Shimizu, Y., Tobiba, R., Hijikata, M., Takaku, H., Shimotohno, K., 2009. Genetic analysis of Hepatitis C virus with defective genome and its infectivity in vitro. J. Virol. 83, 6922–6928.

Suzuki, K., Nakamura, K., Iwata, Y., Sekine, Y., Kawai, M., Sugihara, G., Tsuchiya, K.J., Suda, S., Matsuzaki, H., Takei, N., Hashimoto, K., Mori, N., 2008. Decreased

expression of reelin receptor VLDLR in peripheral lymphocytes of drug-naïve schizophrenic patients. Schizophrenia Res. 98, 148–156.
Thomssen, R., Bonk, S., Propfe, C., Heermann, K.-H., Köchel, H.G., Uy, A., 1992. Association of hepatitis C virus in human sera with b-lipoprotein. Med. Microbiol. Immunol. 181, 293–300.
Thomssen, R., Bonk, S., Thiele, A., 1993. Density heterogeneities of hepatitis C virus in human sera due to the binding of β-lipoproteins and immunoglobulins. Med. Microbiol. Immunol. 182, 329–334.
Thomssen, R., Bonk, S., 2002. Virolytic action of lipoprotein lipase on hepatitis C virus in human sera. Med. Microbiol. Immunol. 191, 17–24.

JOURNAL OF VIROLOGY, Nov. 2010, p. 11761–11770 Vol. 84, No. 22
0022-538X/10/$12.00 doi:10.1128/JVI.00638-10

Sphingomyelin Activates Hepatitis C Virus RNA Polymerase in a Genotype-Specific Manner▽†

Leiyun Weng,[1] Yuichi Hirata,[2] Masaaki Arai,[3] Michinori Kohara,[2] Takaji Wakita,[4] Koichi Watashi,[4,5] Kunitada Shimotohno,[5,6] Ying He,[7] Jin Zhong,[7] and Tetsuya Toyoda[1]*

Units of Viral Genome Regulation[1] and Viral Hepatitis,[7] Institut Pasteur of Shanghai, Key Laboratory of Molecular Virology and Immunology, Chinese Academy of Sciences, 411 Hefei Road, 200025 Shanghai, People's Republic of China; Department of Microbiology and Cell Biology, Tokyo Metropolitan Institute of Medical Biology, 3-18-22 Honkomagome, Bunkyo-Ku, Tokyo 113-8613, Japan[2]; Pharmacology Laboratory, Pharmacology Department V, Mitsubishi Tanabe Pharma Corporation, 1000 Kamoshida-cho, Aoba-ku, Yokohama 227-0033, Japan[3]; Department of Virology II, National Institute of Health, 1-23-1 Toyama, Shinjuku, Tokyo 132-8640, Japan[4]; Laboratory of Human Tumor Viruses, Department of Viral Oncology, Institute for Virus Research, Kyoto University, Kyoto 606-8507, Japan[5]; and Chiba Institute of Technology, 2-17-1 Tsudamuna, Narashino, Chiba 275-0016, Japan[6]

Received 25 March 2010/Accepted 27 August 2010

Hepatitis C virus (HCV) replication and infection depend on the lipid components of the cell, and replication is inhibited by inhibitors of sphingomyelin biosynthesis. We found that sphingomyelin bound to and activated genotype 1b RNA-dependent RNA polymerase (RdRp) by enhancing its template binding activity. Sphingomyelin also bound to 1a and JFH1 (genotype 2a) RdRps but did not activate them. Sphingomyelin did not bind to or activate J6CF (2a) RdRp. The sphingomyelin binding domain (SBD) of HCV RdRp was mapped to the helix-turn-helix structure (residues 231 to 260), which was essential for sphingomyelin binding and activation. Helix structures (residues 231 to 241 and 247 to 260) are important for RdRp activation, and 238S and 248E are important for maintaining the helix structures for template binding and RdRp activation by sphingomyelin. 241Q in helix 1 and the negatively charged 244D at the apex of the turn are important for sphingomyelin binding. Both amino acids are on the surface of the RdRp molecule. The polarity of the phosphocholine of sphingomyelin is important for HCV RdRp activation. However, phosphocholine did not activate RdRp. Twenty sphingomyelin molecules activated one RdRp molecule. The biochemical effect of sphingomyelin on HCV RdRp activity was virologically confirmed by the HCV replicon system. We also found that the SBD was the lipid raft membrane localization domain of HCV NS5B because JFH1 (2a) replicon cells harboring NS5B with the mutation A242C/S244D moved to the lipid raft while the wild type did not localize there. This agreed with the myriocin sensitivity of the mutant replicon. This sphingomyelin interaction is a target for HCV infection because most HCV RdRps have 241Q.

Hepatitis C virus (HCV) has a positive-stranded RNA genome and belongs to the family *Flaviviridae* (21). HCV chronically infects more than 130 million people worldwide (34), and HCV infection often induces liver cirrhosis and hepatocellular carcinoma (19, 28). To date, pegylated interferon (PEG-IFN) and ribavirin are the standard treatments for HCV infection. However, many patients cannot tolerate their serious side effects. Therefore, the development of new and safer therapeutic methods with better efficacy is urgently needed.

Lipids play important roles in HCV infection and replication. For example, the HCV core associates with lipid droplets and recruits nonstructural proteins and replication complexes to lipid droplet-associated membranes which are involved in the production of infectious virus particles (24). HCV RNA replication depends on viral protein association with raft membranes (2, 30). The association of cholesterol and sphingolipid with HCV particles is also important for virion maturation and infectivity (3). The inhibitors of the sphingolipid biosynthetic pathway, ISP-1 and HPA-12, which specifically inhibit serine palmitoyltransferase (SPT) (23) and ceramide trafficking from the endoplasmic reticulum (ER) to the Golgi apparatus (37), suppress HCV virus production in cell culture but not viral RNA replication by the JFH1 replicon (3). Other serine SPT inhibitors (myriocin and NA255) inhibit genotype 1b replication (4, 29, 33). Very-low-density lipoprotein (VLDL) also interacts with the HCV virion (15).

Sakamoto et al. reported that sphingomyelin bound to HCV RNA-dependent polymerase (RdRp) at the sphingomyelin binding domain (SBD; amino acids 230 to 263 of RdRp) to recruit HCV RdRp on the lipid rafts, where the HCV complex assembles, and that NA255 suppressed HCV replication by releasing HCV RdRp from the lipid rafts (29). In the present study, we analyzed the effect of sphingomyelin on HCV RdRp activity *in vitro* and found that sphingomyelin activated HCV RdRp activity in a genotype-specific manner. We also determined the sphingomyelin activation domain and the activation mechanism. Finally, we confirmed our biochemical data by a HCV replicon system.

* Corresponding author. Mailing address: Unit of Viral Genome Regulation, Institut Pasteur of Shanghai, Chinese Academy of Sciences, 411 Hefei Road, 200025 Shanghai, People's Republic of China. Phone and fax: 86 21 6385 1621. E-mail: ttoyoda@amber.plala.or.jp.

† Supplemental material for this article may be found at http://jvi.asm.org.

▽ Published ahead of print on 15 September 2010.

MATERIALS AND METHODS

HCV RNA polymerase. A C-terminal 21-amino-acid deletion was made to the HCV RdRps of strains HCR6 (genotype 1b) (36), NN (1b) (35), Con1 (1b) (5), JFH1 (2a) (36), J6CF (2a) (25), H77 (1a) (7), and RMT (1a), and the mutants

were purified from bacteria as described previously (36). HCR6 (1b) RdRp with the mutation L245A [RdRp(L245A)] or I253A [RdRp(I253A)] or the double mutation L245A and I253A [RdRp(L245A/I253A)]; JFH1 (2a) RdRp with the mutation(s) A242C/S244D, A242, S244D, or T251Q; J6CF (2a) RdRp with the mutation(s) R241Q, S244D, or R241Q/S244D; and H77 (1a) RdRp(A238S/Q248E) were introduced using an *in vitro* mutagenesis kit (Stratagene) and the oligonucleotides listed in Table S1 in the supplemental material. HCR6 (1b) His_6-tagged RdRp(L245A/I253A) was removed from pET21b/KM (36) and cloned into the BamHI/XhoI site of pGEX-6P-3 (GE), resulting in pGEXHCVHCR6RdRp(L245A/I253A).

***In vitro* HCV transcription.** *In vitro* HCV transcription was performed as described previously (36). Briefly, following 30 min of preincubation without ATP, CTP, or UTP, 100 nM HCV RdRp was incubated in 50 mM Tris-HCl (pH 8.0), 200 mM monopotassium glutamate, 3.5 mM $MnCl_2$, 1 mM dithiothreitol (DTT), 0.5 mM GTP, 50 μM ATP, 50 μM CTP, 5 μM [α-^{32}P]UTP, 200 nM RNA template (SL12-1S), 100 U/ml human placental RNase inhibitor, and the lipid (amount indicated below) at 29°C for 90 min. ^{32}P-labeled RNA products were subjected to 6% polyacrylamide gel electrophoresis (PAGE) containing 8 M urea. The resulting autoradiograph was analyzed with a Typhoon Trio plus image analyzer (GE).

RNA filter binding assay. An RNA filter binding assay was performed as described previously (36). Briefly, 100 nM HCV RdRp and 100 nM ^{32}P-labeled RNA template (SL12-1S) were incubated with or without 0.01 mg/ml egg yolk sphingomyelin in 25 μl of 50 mM Tris-HCl (pH 7.5), 200 mM monopotassium glutamate, 3.5 mM $MnCl_2$, and 1 mM DTT at 29°C for 30 min. After incubation, the solutions were diluted with 0.5 ml of TE (50 mM Tris-HCl [pH 7.5], 1 mM EDTA) buffer and filtered through nitrocellulose membranes (0.45-μm pore size; Millipore). The filter was washed five times with TE buffer, and the bound radioisotope was analyzed by Typhoon Trio plus after being dried.

Enzyme-linked immunosorbent assay (ELISA). Ninety-six-well microtiter plates (Corning) were coated with 250 ng of egg yolk sphingomyelin in ethanol by evaporation at room temperature. After the wells were blocked with phosphate-buffered saline (PBS) and 3% bovine serum albumin (BSA), they were incubated with 1 pmol of the HCV RdRp of HCR6 (1b) wild type (wt) or L245A, I253A, or L245A/I253A mutant; NN (1b); H77 (1a); RMT (1a); J6CF (2a); or JFH1 (2a) wt or A242C/S244D, A242, S244D, or T251Q mutant in Tris-buffered saline (50 mM Tris-HCl [pH 7.5] and 150 mM NaCl) for 1.5 h at room temperature. After being blocked with 3% BSA, the bound HCV RdRp was detected by adding rabbit anti-HCV RdRp serum (1:5,000) (see Fig. S1 in the supplemental material) (17) before incubation with a horseradish peroxidase (HRP)-conjugated anti-rabbit IgG antibody (1:5,000; Southern Biotech). The optical density at 450 nm (OD_{450}) was measured with a Spectra Max 190 spectrophotometer (Molecular Devices) using a TMB (3,3′,5,5′-tetramethylbenzidine) Liquid Substrate System (Sigma).

HCV subgenomic replicon. A D244S mutation was introduced into the HCV strain NN (1b) subgenomic replicon pLMH14 (35), resulting in pLMH(NN)5B(D244S) [where 5B(D244S) is the NS5B protein with the mutation D244S]. The A242C/S244D mutation was introduced into the HCV JFH1 (2a) replicon, pSGR-JFH1/luc (25), resulting in pSGR-JFH1/luc5B(A242C/S244D). The HpaI and XbaI fragment of pSGR-JFH1 (18) was replaced with that of pSGR-JFH1/luc5B(A242C/S244D), resulting in pSGR-JFH15B(A242C/S244D). The A238S/Q248E mutation was introduced into HCV H77 (1a) replicon pHCVrep13(S2204I)/Neo (7) after the neomycin gene was replaced by the firefly luciferase gene [pH77(I)/luc] by insertion of AflII and AscI sites (see Table S1 in the supplemental material), resulting in pH77(I)/luc5B(A238S/Q248E). Subgenomic replicon RNA was transcribed *in vitro* by T7 RNA polymerase using MegaScript (Ambion) after the replicon plasmids were linearized by XbaI (strain NN and JFH1 replicons) or HpaI (strain H77 replicon). Subgenomic replicon RNA was stored at −80°C after being purified by phenol-chloroform extraction and ethanol precipitation.

Replicon assay with myriocin. Huh7.5.1 cells were kindly provided by F. Chisari and were maintained in Dulbecco's modified Eagle's medium (DMEM; Gibco) with 10% fetal bovine serum (FBS; Gibco) (38). HCV replicon RNA (10 μg) was transfected into 4×10^6 Huh7.5.1 cells (1×10^7/ml) in OptiMEM I (Gibco) by electroporation (GenePulser Xcell; Bio-Rad) at 270 V, 100 Ω, and 950 μF. After transfection, the cells were plated in 12-well plates incubated in DMEM–10% FBS. At 6 h after transfection, cells were treated with 0, 5, and 50 nM myriocin. At 4, 54, and 78 h after transfection (48 and 72 h after myriocin treatment), the cells were harvested, and luciferase activity was measured using a Dual-Glo luciferase assay kit and a GloMax 96 Microplate Luminometer (Promega). Luciferase activity was normalized against the activity at 4 h after transfection (26).

HCV JFH1 wt and NS5B(A242C/S244D) replicon cells. Huh7/scr cells were kindly provided by F. Chisari of the Scripps Research Institute and were maintained in Dulbecco's modified Eagle's medium (Gibco) with 10% fetal bovine serum (Gibco). RNA (10 μg each) from SGR-JFH1 and SGR-JFH1 with the mutations A242C/S244D in NS5B [NS5B(A242C/S244D) was transfected into 4×10^6 Huh7/scr cells (1×10^7/ml) in OptiMEM I (GIBCO) by electroporation (GenePulser Xcell; Bio-Rad) at 270 V, 100 Ω, and 950 μF. After transfection, the cells were plated in 10-cm dishes and incubated in DMEM–10% FBS with 1.0 and 0.5 mg/ml G418 (Gibco). JFH1 wt and NS5B(A242C/S244D) replicon cells were maintained in DMEM–10% FBS and 0.5 mg/ml G418.

Membrane floating assay. JFH1 wt and NS5B(A242C/S244D) replicon cells were suspended in two packed cell volumes of hypotonic buffer (10 mM HEPES-NaOH [pH 7.6], 10 mM KCl, 1.5 mM $MgCl_2$, 2 mM DTT, and 1 tablet/25 ml of EDTA-free protease inhibitor cocktail tablets [Roche]) and disrupted by 30 strokes of homogenization in a Dounce homogenizer using a tight-fitting pestle at 4°C. After nuclei were removed by centrifugation at 2,000 rpm for 10 min at 4°C, the supernatant (postnuclear supernatant [PNS]) was treated with 1% Triton X-100 in TNE buffer (25 mM Tris-HCl [pH 7.6] 150 mM NaCl, 1 mM EDTA) for 30 min on ice. The lysates were supplemented with 40% sucrose and centrifuged at 38,000 rpm in a Beckman SW41 Ti rotor (Beckman Coulter) overlaid with 30% and 10% sucrose in TNE buffer at 4°C for 14 h.

Western blotting. Western blotting using anti-HCV RdRp (17), rabbit anti-NS3 (32), anti-NS5A (16) and anti-caveolin-2 was performed as previously published (17).

Reagent. Egg yolk sphingomyelin, cholesterol phosphocholine, myriocin, and rabbit anti-caveolin-2 antibodies were purchased from Sigma. Hexanoyl sphingomyelin, C_6-ceramide, C_8-β-D-glucosyl ceramide, and C_8-β-D-lactosyl ceramide were purchased from Avanti Polar Lipids. [α-^{32}P]UTP was purchased from New England Nuclear.

Statistical analysis. Significant differences were evaluated using *P* values calculated from a Student's *t* test.

Nucleotide sequence accession number. The sequence of HCV RMT has been deposited in the GenBank under accession number AB520610.

RESULTS

Sphingomyelin activation of HCV RNA polymerases of various genotypes. There are several sequence variations in the sphingomyelin binding domain (SBD; amino acids 231 to 260 of HCV RdRp) among HCV genotypes (see Fig. 7A). In order to compare the RdRps of different genotypes of HCV, we purified RdRp from genotypes 1b (strains HCR6, NN, and Con1), 1a (H77 and MRT), and 2a (JFH1 and J6CF) (see Fig. S2 in the supplemental material). First, the effect of ethanol on HCV HCR6 (1b) RdRp transcription was examined because lipids were suspended in ethanol before they were added to the HCV transcription reaction mixture. We found that 2% ethanol did not inhibit HCV transcription (see Fig. S3 in the supplemental material); therefore, all subsequent experiments were performed using less than 2% ethanol.

The kinetics of sphingomyelin activation were analyzed using egg yolk sphingomyelin for HCR6 (1b) RdRp wt (Fig. 1A) and subtype 2a (JFH1 and J6CF) RdRps (Fig. 1B), and *N*-hexanoyl-D-*erythro*-sphingosylphosphorylcholine (hexanoyl sphingomyelin) was used for HCR6 (1b) RdRp wt (Fig. 1C) and subtype 1a (H77 and RMT) RdRps (Fig. 1D). The egg yolk sphingomyelin activation curve of HCR6 (1b) RdRp wt at low concentrations (<0.01 mg/ml) was sigmoid. The transcription activity of HCR6 (1b) RdRp wt increased in a dose-dependent manner. It was activated 11-fold at 0.01 mg/ml and then plateaued (14-fold activation) at 0.1 mg/ml. However, JFH1 (2a) and J6CF (2a) RdRps were activated 2.5-fold and 2.2-fold, respectively, at 0.01 mg/ml sphingomyelin, at which point they plateaued.

Egg yolk sphingomyelin is a mixture. In order to obtain the optimal molar ratio for sphingomyelin activation of HCR6 (1b)

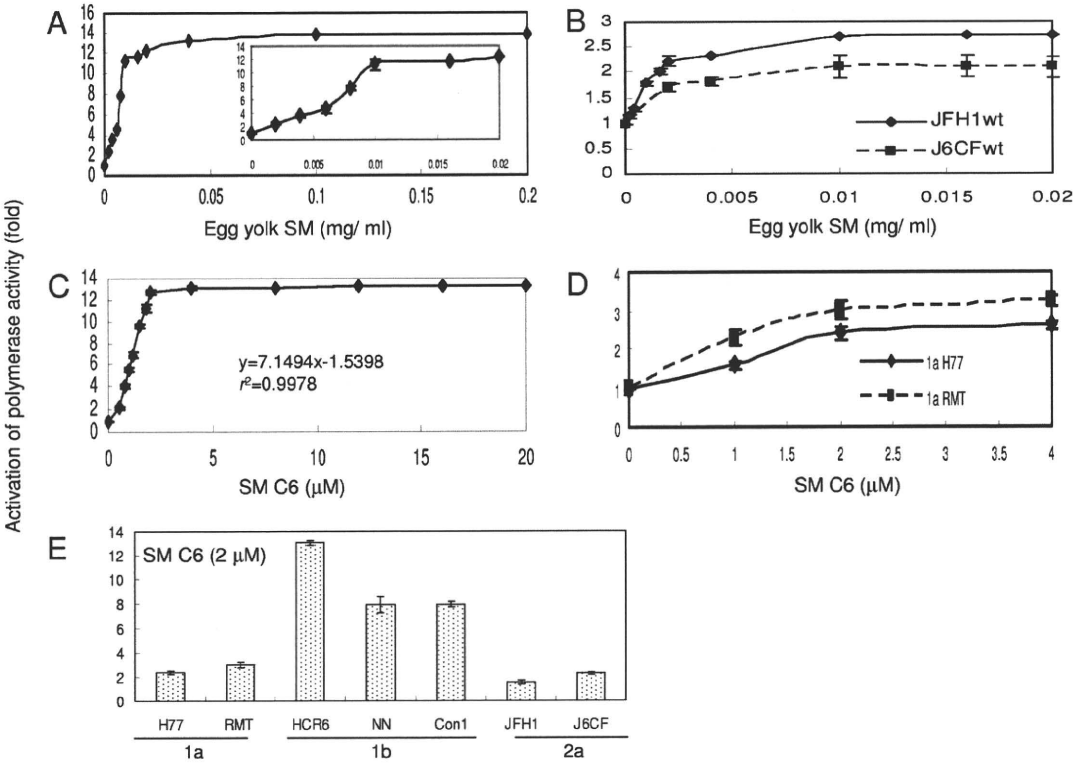

FIG. 1. Sphingomyelin activation of HCV RNA polymerases. (A) Activation kinetics of HCV HCR6 (1b) RdRp wt by egg yolk sphingomyelin (SM). The inset shows activation produced by 0 to 0.02 mg/ml egg yolk sphingomyelin. Activation kinetics of HCV 2a (JFH1 and J6CF) RdRps by egg yolk sphingomyelin (B) and of HCV HCR6 (1b) RdRp wt by hexanoyl sphingomyelin (SM C6) (C). In panel C, the first order of the graph was fitted by linear regression; the calculated equation is indicated in the graph. (D) Activation kinetics of HCV 1a (H77 and RMT) RdRps by hexanoyl sphingomyelin. (E) Activation effect of hexanoyl sphingomyelin on HCV RdRp of various genotypes. HCV RdRp (100 nM) was incubated with or without 2 μM SM C6. The names of the RdRps are indicated below the graph. Mean ± standard deviation of the activation ratio was calculated from three independent experiments.

RdRp wt, its activation kinetics were calculated using hexanoyl sphingomyelin (Fig. 1C, SM C6). The equation for the first-order ratio of hexanoyl sphingomyelin activation according to linear regression fitting was as follows: $y = 7.1494x - 1.5398$, where y is the activation ratio and x is the sphingomyelin concentration ($r^2 = 0.9978$). RdRp activation had almost plateaued at 2 μM hexanoyl sphingomyelin. The activation kinetics of JFH1 (2a) and J6CF (2a) RdRps in egg yolk sphingomyelin were biphasic and plateaued at 0.01 mg/ml. Those of RMT (1a) and H77 (1a) RdRps in hexanoyl sphingomyelin were also biphasic and plateaued at 2 μM. The curve of the first order was fitted by linear regression. The molar ratio of RdRp to hexanoyl sphingomyelin at its plateau was calculated as 1:20.

Because RdRp activation had almost plateaued at 2 μM hexanoyl sphingomyelin, we compared the effect of sphingomyelin on 100 M concentrations of RNA polymerases of the HCV 1a, 1b, and 2a genotypes using 2 μM hexanoyl sphingomyelin (Fig. 1E and Table 1).

Helix-turn-helix structure for sphingomyelin binding and activation. Sphingomyelin binds to the SBD peptide (see HCV SBD in Fig. 7) (29). Initially, we tested whether SBD was the sphingomyelin binding site in HCV RdRp by ELISA (Fig. 2A and Table 1). When the L245 and I253 residues of the SBD peptide were mutated to A, sphingomyelin binding activity was lost (29). We introduced the same mutations in HCV HCR6 (1b) RdRp and purified HCR6 (1b) RdRp with mutations L245A, I253A, and L245A/I253A. Because the C-terminal His-tagged HCR6 RdRp(L245A/I253A) was not soluble, it was solubilized by tagging of glutathione *S*-transferase (GST) sequence at the N terminus but lost polymerase activity. As the L245A/I253A mutant had lost its polymerase activity, polymerase activation was tested only for L245A and I253A (Fig. 2B and Table 1). These results confirmed that SBD located in the finger domain (residues 230E to 263G) successfully achieved sphingomyelin binding in HCV RdRp and that sphingomyelin did not bind to the SBD when the helix-turn-helix structure had been destroyed by the L245A or I253A mutation (29).

The sphingomyelin binding activities of genotype 1a and 2a RdRps were also tested (Fig. 2 and Table 1). Both JFH1 and J6CF were tested for genotype 2a because J6CF (2a) RdRp had an additional amino acid difference at position 241 in the SBD, and its sphingomyelin binding activity was very low (Fig. 2A and 7A; Table 1). J6CF (2a) RdRp(R241Q) showed the same sphingomyelin binding activity as HCR6 (1b) RdRp wt, indicating that 241Q was the critical amino acid for sphingomyelin binding. J6CF (2a) RdRp(S244D) and RdRp(R241Q/S244D) also showed higher sphingomyelin binding activity

TABLE 1. Summary of sphingomyelin activation of HCV RNA polymerase activities

Parameter	Value for the parameter by RdRp genotype, strain, and variant[a]																				
	1b								1a				2a								
	HCR6												J6CF				JFH1				
	wt	L245A	I253A	L245A/I253A	D244S	NN	Con1	RMT	wt	H77 A238S/Q248E	wt	R241Q	S244D	R241Q/S244D	wt	A242C	S244D	A242C/S244D	T251Q
SM binding (%)[b]	100	24.3	30.8	15.5	78.7	93.4	117	144	86.7	82.5	19.3	118	53.1	80.2	70.4	75.5	93.1	92.4	80.7
Activation of polymerase (*n*-fold)[c]	13.0 (11.2)[d]	(2.8)[d]	(2.5)[d]	ND	3.6	7.9	7.9	3.0	2.0	8.1	2.3	4.3	5.6	3.4	1.6	1.0	3.1	4.4	1.8
Activation of RNA binding (*n*-fold)[c]	4.5	2.6	1.7	ND	1.9	ND	ND	ND	1.4	3.3	1.5	3.6	3.2	1.7	1.3	ND	ND	1.4	ND

[a] Numbers were averaged from three independent experiments. ND, not done.
[b] Egg yolk sphingomyelin (SM; 250 ng) was used.
[c] Hexanoyl sphingomyelin (2 μM) was used.
[d] Egg yolk sphingomyelin (0.01 mg/ml) was used.

than the wt ($P < 0.001$) but lower binding than the R241Q mutant. However, S244D showed higher RdRp activation than R241Q ($P < 0.005$), while the RdRp activation ratio of the double mutant (R241Q/S244D) was lower than that of S244D or R241Q, although all of them activated RdRp with sphingomyelin ($P < 0.005$) (Fig. 2A and C and Table 1). For JFH1, when the JFH1 RdRp SBD was modified (A242C/S244D) to allow it to bind with more sphingomyelin than the wt ($P < 0.005$), the mutant JFH1 RdRp(A242C/S244D) was activated more than the wt by sphingomyelin ($P < 0.005$) (Fig. 2A and C; Table 1). The sphingomyelin binding activity of JFH1 RdRp(T251Q) was 80.7% of that of HCR6 (1b), and its activation ratio was 1.8-fold. These results agree that SBD is both the sphingomyelin activation and binding domain and that the domains for these two activities are somehow different.

We determined which amino acid, 242C or 244D, enhanced sphingomyelin binding by comparing HCR6 (1b) and JFH1 (2a) RdRps. Sphingomyelin binding of HCR6 (1b) RdRp(D244S) was 79% of that of the wt ($P < 0.005$) (Fig. 2A and Table 1), and its activation by sphingomyelin was only 3.6-fold (Fig. 2C and Table 1). The sphingomyelin binding of JFH1 (2a) RdRp(A242C) and RdRp(S244D) increased to 75.5% and 93.1%, respectively, of HCR6 (1b) RdRp wt (Fig. 2A and Table 1). This was significantly higher than that of JFH1 (2a) RdRp wt ($P < 0.005$), and the sphingomyelin activation of JFH1 (2a) RdRp(A242C) and RdRp(S244D) was increased 1.0-fold and 3.1-fold, respectively ($P < 0.005$) (Fig. 2C and Table 1). From these mutation analyses of the J6CF and JFH1 RdRps, we concluded that 244D enhanced sphingomyelin binding and RdRp activation.

HCV 1a RdRps were not activated even though sphingomyelin bound to them (Fig. 1E and 2A and Table 1). We then tried to elucidate the domains responsible for sphingomyelin activation. There are 14 amino acids (residues 19, 25, 81, 111, 120, 131, 184, 270, 272, 329, 436, 464, 487, and 540) unique to genotype 1a RdRp in the region of residues 1 to 570 and two amino acid differences unique to 1a RdRp in SBD, i.e., 238A and 248Q (see Fig. 6A). Initially, we focused on the SBD and introduced the A238S and Q248E mutations into the H77 (2a) RdRp SBD (Fig. 2A and D and Table 1). The sphingomyelin binding activity of H77 (2a) RdRp(A238S/Q248E) was similar to that of H77 (2a) RdRp wt. The sphingomyelin activation ratio of H77 (2a) RdRp(A238S/Q248E) was increased 8.1-fold, leading us to conclude that these mutations are essential to sphingomyelin activation.

Effect of lipids on HCV RNA polymerase activity. In order to elucidate the structure of the lipids involved in activation of HCV RdRp, D-lactosyl-β-1,1′-*N*-octanoyl-D-*erythro*-sphingosine [C_8-lactosyl(β) ceramide], D-glucosyl-β1-17-N-octanoyl-D-*erythro*-sphingosine (C_8-β-D-glucosyl ceramide), *N*-hexanol-D-*erythro*-sphingosine (C_6-ceramide), and cholesterol were tested for their abilities to activate RdRp. The relative polymerase activities of 100 nM HCV HCR6 (1b) RdRp activated with 0.01 mg/ml egg yolk sphingomyelin, 2 μM hexanoyl sphingomyelin, 8 μM C_8-lactosyl(β) ceramide, 12 μM C_8-β-D-glucosyl ceramide, 12 μM C_6-ceramide, and 0.02 mg/ml cholesterol were 11.2, 13.0, 5.66, 4.19, 1.12, and 2.25 of that without lipids, respectively (Fig. 3A). The amount of lipids that gave the maximum activation was calculated from the kinetics of the lipids bound to HCR6 (1b) and JFH1 (2a) RdRps (Fig. 3B and

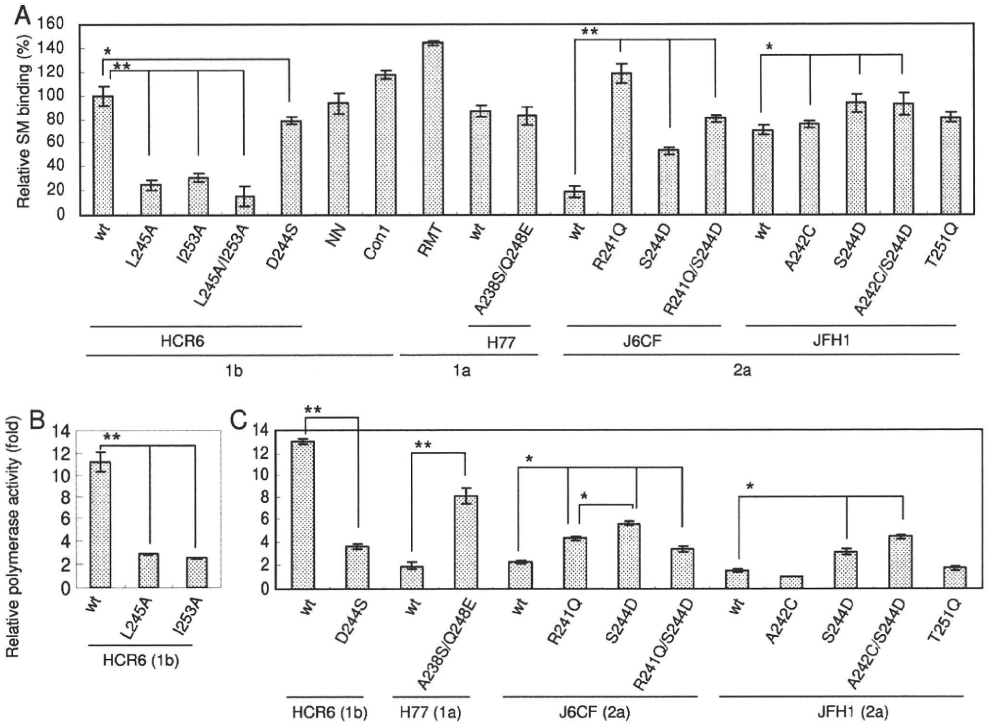

FIG. 2. Sphingomyelin binding and activation of HCV RNA polymerase sphingomyelin binding domain mutants. Names of RdRps are indicated below the graphs. (A) Egg yolk sphingomyelin (SM) binding activity relative to that of HCR6 (1b) RdRp wt. Mean ± standard deviation of the binding was calculated from three independent experiments. (B) Egg yolk sphingomyelin activation of HCR6 (1b) RdRps. RdRps (100 nM) were incubated with or without 0.01 mg/ml egg yolk sphingomyelin. (C) Hexanoyl sphingomyelin activation of the RdRps (RdRp names are indicated below the graphs). HCV RdRps (100 nM) were incubated with or without 2 μM hexanoyl sphingomyelin. The mean ± standard deviation of the activation ratio was calculated from three independent experiments. *, $P < 0.005$; ** $P < 0.001$.

C). C_8-lactosyl(β) ceramide and C_8-β-D-glucosyl ceramide activated HCR6 (1b) RdRp compared with the linear regression kinetics of the reaction with hexanoyl sphingomyelin as it plateaued (Fig. 1C and 3B). Cholesterol activated HCR6 (1b) RdRp slightly but did not activate JFH1 (2a) RdRp (Fig. 3C). We therefore concluded that the phosphocholine of sphingomyelin bound to the SBD of HCV RdRp because the order of HCV RdRp activation was hexanoyl sphingomyelin > C_8-lactosyl(β) ceramide > C_8-β-D-glucosyl ceramide, and C_6-ceramide did not activate HCV HCR6 (1b) RdRp. The polarity of the phosphocholine of sphingomyelin is important for HCV RdRp activation (see Fig. S5 in the supplemental material).

In order to test whether phosphocholine activated HCV RdRp (Fig. 3D), HCR6 (1b) RdRp was incubated with 0.4, 2, 20, 100, and 400 μg and 2, 4, 11, 54, and 100 mg of phosphocholine. Up to 400 μg of phosphocholine did not affect RdRp activity, but more than 2 mg of phosphocholine inhibited RdRp activity.

Effect of sphingomyelin on the template RNA binding of HCV RNA polymerase. The mechanism of HCV RdRp activation was analyzed. RNA polymerase changes its conformation throughout the different transcription steps, and template binding is the first step of transcription (9). Therefore, the effect of sphingomyelin on template RNA binding activity was tested (Fig. 4A and Table 1). Sphingomyelin enhanced the template RNA binding of HCR6 (1b) RdRp wt but not that of JFH1 (2a), H6CF (2a), or H77 (1a) wt RdRp. When the A238S/Q248E mutation was introduced into H77 (1a) RdRp, the RNA binding was enhanced. J6CF (2a) RdRp R241Q and S244D mutants showed similar enhancement of RNA binding, but the R241Q/S244D double mutant did not. The activation effect of RNA binding of HCR6 (1b) RdRp mutants L245A, I253A, and D244S was lower than that of RdRp wt. JFH1 (2a) RdRp wt and RdRp(A242C/S244D) showed similar RNA binding activation levels. Based on a comparison of the sphingomyelin activation of HCR6 (1b) RdRp wt and its mutants which lost sphingomyelin binding with J6CF (2a) RdRp wt and the R241Q and S244D mutants and H77 (1a) RdRp wt and the A238S/Q248E mutant, we concluded that polymerase activation by sphingomyelin was induced mainly via activation of the template RNA binding of RdRp. RNA binding activity of JFH1 (2a) RdRp wt and RdRp(A242C/S244D) was almost saturated because RNA binding of these RdRps was not activated by sphingomyelin (see Fig. S4 in the supplemental material).

HCV RdRp has to be bound with sphingomyelin before or at the same time as it binds to template RNA. After RdRp had bound to the template RNA, sphingomyelin did not enhance template RNA binding strongly (Fig. 4B).

Effect of the sphingomyelin binding domain mutations for HCV replicon activity with myriocin. In order to confirm sphingomyelin activation of HCV polymerase activity in a viral replication system, HCV replicon activity of the loss-of-function mutant HCV NN (1b) NS5B(D244S) and the gain-of-

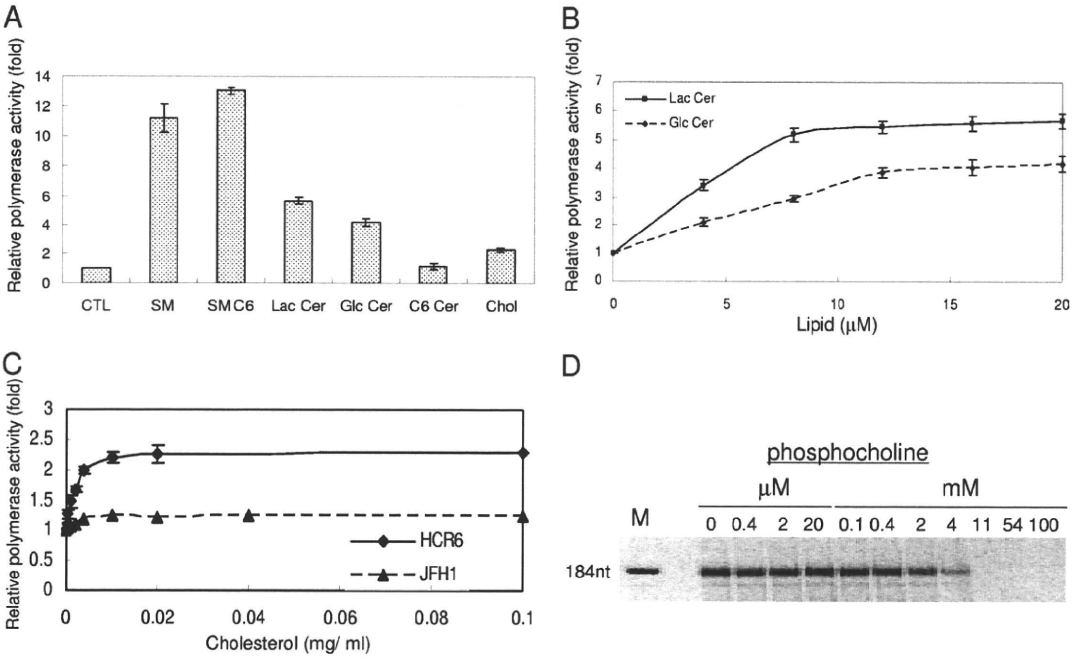

FIG. 3. HCV RNA polymerase activation effect of lipids. (A) Lipid activation of HCR6 (1b) RdRp wt. HCV HCR6 (1b) RdRp wt (100 nM) was incubated with or without (control [CTL]) 0.01 mg/ml egg yolk sphingomyelin (SM), 2 μM hexanoyl sphingomyelin (SM C6), 8 μM C_8-lactosyl(β) ceramide (Lac Cer), 12 μM C_8-β-D-glucosyl ceramide (Glc Cer), 12 μM C_6-ceramide (C6 Cer), or 0.02 mg/ml cholesterol (chol). (B) Activation kinetics of C_8-lactosyl(β) ceramide (Lac Cer) and C_8-β-D-glucosyl ceramide (Glc Cer) on HCR6 (1) RdRp. (C) Activation kinetics of cholesterol on HCR6 (1b) and JFH1 (12a) RdRps. (D) The effect of phosphocholine on HCR6 (1b) RdRp. The mean ± standard deviation of the activation ratio was calculated from three independent experiments.

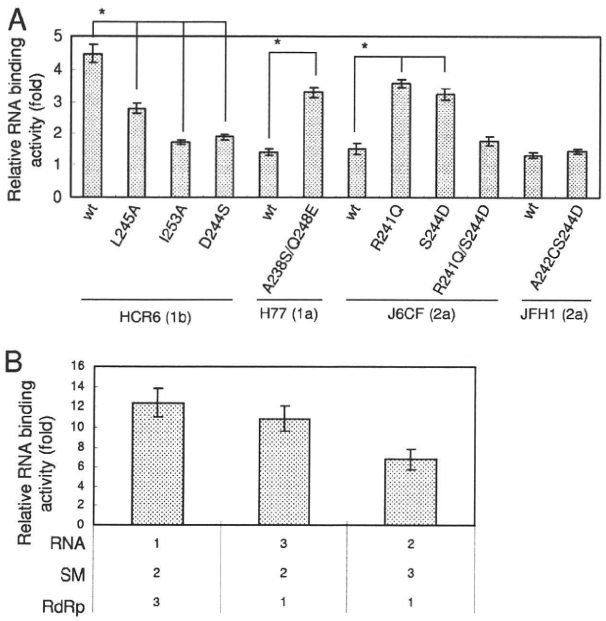

FIG. 4. Sphingomyelin activation of the RNA binding activity of HCV RNA polymerase. (A) Sphingomyelin activation of RNA filter binding of HCV RdRps (RdRp names are indicated below the graph). RdRps and ^{32}P-labeled RNA template (SL12-1S) were incubated with or without egg yolk sphingomyelin (SM), before filtration. (B) Effect of the order of sphingomyelin treatment. Numbers below the graph indicate the order in which the reagents were added. The graph represents the ratio to RNA binding without sphingomyelin. The mean ± standard deviation of the activation ratio was calculated from three independent experiments. *, $P < 0.01$.

function mutants H77 (1a) NS5B(A238S/Q248E) and JFH1 (2a) NS5B(A242C/S244D) were compared with 5 and 50 nM myriocin treatment for 72 h (Fig. 5).

First, HCV replicon activity was compared as the relative luciferase activity (Fig. 5A). Both JFH1 (2a) wt and NS5B(A242C/S244D) replicons showed similar and strong replicon activity ($133 \times 10^3 \pm 12 \times 10^3$ and $138 \times 10^3 \pm 8.5 \times 10^3$, respectively). JFH1 (2a) wt replicon was resistant to myriocin treatment, as reported by Aizaki et al. using other SPT inhibitors (3). The JFH1 (2a) NS5B(A242C/S244D) replicon became sensitive to myriocin but still showed higher replicon activity than NN (1b) or H77 (1a) replicons even at 50 nM myriocin.

To analyze the effect of mutations precisely, the replicon activity relative to each wt strain was compared (Fig. 5B). The JFH1 (2a) wt replicon with 50 nM myriocin showed the same luciferase activity as the wt without myriocin (102% ± 9.6%). JFH1 (2a) NS5B(A242C/S244D) replicon activity was the same as that of the wt without myriocin (103% ± 12%); with 5 nM myriocin it was 84.1% ± 6.6% of the wt level, but with 50 nM myriocin it was 70.3% ± 5.3% of the wt level, which was significantly lower ($P < 0.01$). NN (1b) wt replicon activity was 45.3% ± 6.6% with 5 nM myriocin and 21.7% ± 2.9% with 50 nM myriocin relative to the wt level without myriocin. NN (1b) NS5B(D244S) replicon activity was 72.2% ± 12% without myriocin ($P < 0.05$), 44.0% ± 7.4% with 5 nM myriocin, and 38.1% ± 4.2% with 50 nM myriocin relative to wt level without myriocin, which was significantly higher ($P < 0.01$). Thus, NN (1b) NS5B(D244S) showed lower replicon activity than the wt

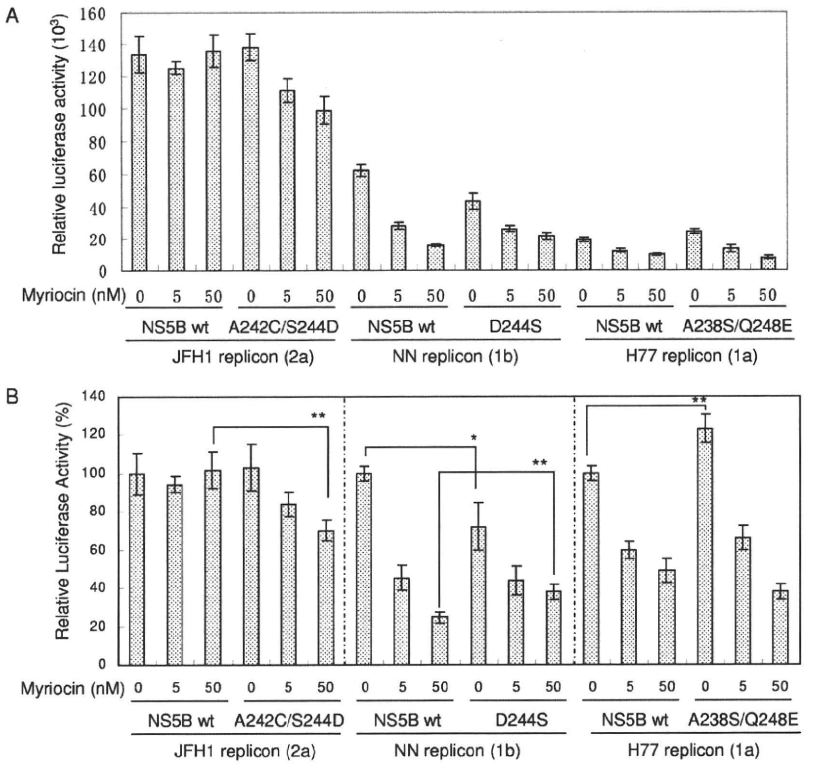

FIG. 5. Myriocin inhibition of HCV replicon activity. Huh7.5.1 cells were incubated with myriocin after transfection with the HCV replicons indicated below the graphs. Means ± standard deviations of the relative luciferase activity at 72 h after myriocin treatment compared to activity at 4 h after transfection (A) and to that of each wt without myriocin (B) were calculated from three independent measurements. *, $P < 0.05$; ** $P < 0.01$.

and was less sensitive to myriocin than the wt. H77 (1a) wt replicon activity was 59.9% ± 4.2% with 5 nM myriocin and 49.2% ± 6.4% with 50 nM myriocin relative to the wt level without myriocin. H77 (1a) NS5B(A238S/Q248E) replicon activity was 123% ± 7.1% without myriocin ($P < 0.01$), 66.1% ± 6.3% with 5 nM myriocin, and 38.0% ± 4.1% with 50 nM myriocin relative to wt level without myriocin. Both H77 (1a) wt and NS5B(A238S/Q248E) replicons were sensitive to myriocin, and the replicon activity of NS5B(A238S/Q248E) was higher than that of the wt.

JFH1 (2a) RdRp(A242C/S244D) localized in the DRM fractions. Myriocin sensitivity of JFH1 (2a) NS5B(A242C/S244D) replicon indicates the importance of 244D in JFH1 NS5B for sphingomyelin binding. To further confirm the role of 244D for recruitment of HCV RdRp to the detergent-resistant membrane (DRM), where the HCV replication complex exists, we compared the distribution of NS5A and NS5B of JFH1 (2a) wt and NS5B(A242C/S244D) in their replicon cells by sucrose density gradient centrifugation of the DRM (Fig. 6). NS5A proteins of both JFH1 (2a) wt and NS5B(A242C/S244D) replicons localized in the DRM fraction where caveolin-2 was present (11, 27), but most of NS5B wt localized in the Triton-soluble fractions. NS5B of JFH1 (2a) NS5B(A242C/S244D) replicon was shifted to the DRM fraction from the soluble fraction. The shift of NS5B(A242C/S244D) localization into the DRM demonstrated that SBD was the DRM localization domain of NS5B and that residue 244D was important for this localization.

DISCUSSION

Hepatitis C virus is an envelope virus, and the lipid components of the virion play important roles in HCV infectivity and virion assembly (3, 15, 20, 24). HCV replication complexes localize in lipid raft structures/DRMs in the membrane frac-

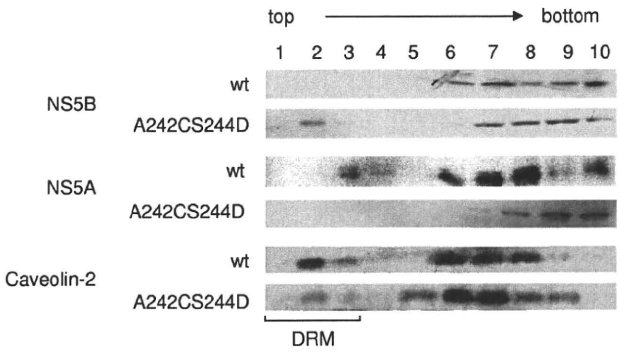

FIG. 6. Membrane floating assay of JFH1 wt and NS5B(A242C/S244D) replicon cells. The PNS fractions of HCV JFH1 (2a) wt and NS5B(A242C/S244D) replicon cells were treated with 1% Triton X-100 in TNE buffer for 30 min at 4°C and subjected to 10 to 40% sucrose gradient centrifugation in TNE buffer. Each fraction was subjected to 10% SDS-PAGE, followed by Western blotting with anti-NS5A, -NS5B, and -caveolin-2 antibodies. Fractions are numbered as indicated at the top of the panel. The DRM fractions (fractions 1 to 3) are indicated.

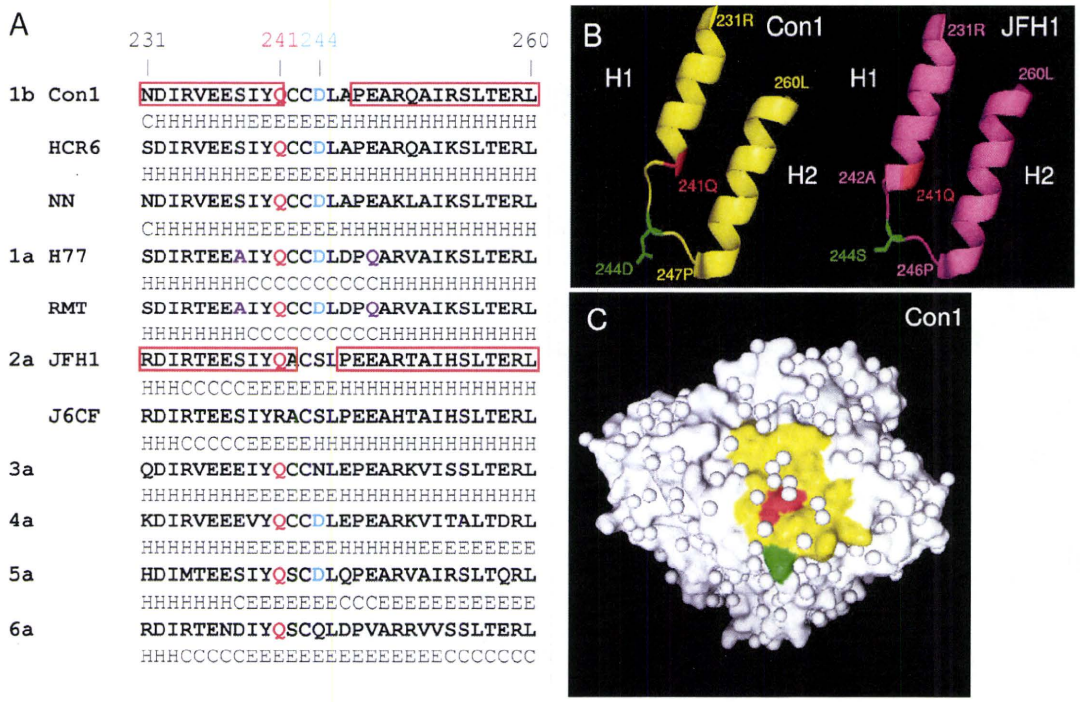

FIG. 7. Sphingomyelin binding domain (SBD) of HCV RNA polymerase. (A) The SBDs (231N to 260L) of HCV RdRps are aligned together with their secondary structure predicted by the Chou-Fasman program (10). The predicted secondary structure is indicated below the sequence as follows: H, α-helix; E, β-sheet; and C, coil. The α-helix structures of HCV Con1 (1b) RdRp and JFH1 (2a) RdRp are boxed in red. Residues 241Q and 244D are indicated in red and green, respectively. The 238A and 248E of the H77 and RMT (1a) RdRps are indicated in purple. GenBank accession numbers of HCV genotypes 3a, 4a, 5a, and 6a are GU814263 (12), GU814265 (12), Y13184 (8), and Y12083 (1), respectively. (B) Comparison of the SBDs of HCV Con1 (1b) (yellow) and JFH1 (2a) RdRps (magenta). The starting and ending amino acids of H1 and H2 are indicated. The sphingomyelin binding site, 241Q, is indicated in red, and 244D of Con1 (1b) and 244S of JFH1 (2a) RdRp are indicated in green. (C) Surface model of HCV Con1 (1b) RdRp. SBD is indicated in yellow, and 241Q and 244D are indicated in red and green, respectively. The structures of the Con1 and JFH1 RdRps were constructed by PyMOL, version 1.1.1 (http://www.pymol.org/). PDB numbers of Con1 (1b) RdRp and JFH1 (2a) RdRp are 3FQL (14) and 3I5K (31), respectively.

tions of subgenomic replicon cells (30). Lipid rafts are composed mainly of sphingomyelin, cholesterol, and glycosphingolipids. Most reports regarding the relationship between lipids and HCV have examined virion assembly, infectivity, and the localization of HCV, but their biochemical interactions have not been reported. Our findings clearly demonstrate that sphingomyelin plays an important role not only in HCV replication complex formation and its localization but also in HCV RdRp activity.

The helix-turn-helix structure of the SBD (residues 230 to 263), which is located between RNA polymerase motifs A and B, has been proposed as the sphingomyelin binding domain of HCV RdRp (29). We compared the SBD of Con1 (1b) (Protein Data Bank [PDB] 3FQL) (14) and JFH1 (2a) (PDB 3I5K) (31) and the secondary structure of the amino acids (201 to 290) in the SBD predicted by the Chou-Fasman program (10) (Fig. 7; see also Fig. S5 in the supplemental material) because the helix structures of the SBD of Con1 (helix 1 [H1], 231N to 241Q; helix 2 [H2], 247A to 260L) and JFH1 (H1, 231R to 242A; H2, 246P to 260L) RdRp fit with those predicted by the Chou-Fasman program. The structures contributing to sphingomyelin binding and activation are H1 and H2 and the junction (turn) between the two helix structures that are similar to the human immunodeficiency virus (HIV) gp120 V3 domain, prion protein (PrP), and β-amyloid peptide (13, 22). Although Con1 (1b) RdRp has a shorter helix structure than JFH1 (2a) RdRp (Fig. 6B), the structures of their SBDs are very similar (Fig. 7; see also Fig. S5). When the helix-turn-helix structure of the SBD was destroyed (HCR6 genotype 1b RdRp mutants L245A and I253A), the RdRp lost sphingomyelin binding activity and lost its activation (Fig. 2).

In order to study the structure-function relationship of the SBD and sphingomyelin, we compared the SBD of genotype 1a, 1b and 2a RdRps and particularly focused on residue 244D in the turn and residues 241Q and 238S/248E in the helix domains. The polar amino acid 241Q and the negatively charged 244D of Con1 (1b) RdRp located on the surface of the RdRp molecule bind and interact with the positively charged choline residue of sphingomyelin (Fig. 7C; see also Fig. S5 in the supplemental material). The positively charged 241R repels the choline residue of sphingomyelin, and as a result, J6CF (a) RdRp wt did not bind to sphingomyelin. J6CF (2a) RdRp(R241Q) showed almost the same sphingomyelin binding activity as HCR6 (1b) RdRp wt. This ionic interaction between SBD and sphingomyelin agrees with the activation of lipids with different sphingosine structures and fatty acid chains (Fig. 3A). JFH1 (2a) RdRp does not interact well with sphingomyelin because it does not have the negatively charged

amino acids at the tip of its turn structure. Once its 244S was changed to D, more sphingomyelin bound to JFH1 (2a) RdRp and activated the RdRp (Fig. 2A and C). The reason for the low activation of J6CF (2a) RdRp(R241Q/S244D) is not clear. Sometimes mutations affect the entire conformation of the molecule. In conclusion, from the comparison of sphingomyelin binding and activation of HCR6 (1b), J6CF (2a), and JFH1 (2a) RdRp SBD mutants, 241Q is the essential amino acid for sphingomyelin binding in the SBD. Amino acid 244D enhanced both binding and RdRp activation.

The *in vitro* sphingomyelin binding and RdRp activation experiments indicate that sphingomyelin binding and its RdRp activation are different biochemical reactions because we found controversial activation rates for sphingomyelin binding and RdRp activation among J6CF (2a) RdRp mutants (Fig. 2). The relationship between sphingomyelin binding and the activation of polymerase activity was studied by comparing genotype 1b and 1a RdRps, both of which bind to sphingomyelin (Fig. 2). However, 1a RdRp is not activated by sphingomyelin because both of the helix structures of 1a RdRp are probably terminated at 238A and 248Q, making its helix structures shorter than those of 1b RdRp (Fig. 6A). The length of the helix structure may be essential for sphingomyelin activation because RdRp changes its structure to bind to template RNA when sphingomyelin binds to SBD (Fig. 4).

HCV RdRp changes its conformations at the early stages of transcription initiation, including the template RNA binding step (6, 9). Sphingomyelin binding is likely to change the conformation of 1b RdRp to recruit template RNA and initiate transcription efficiently. Comparison of the activation ratio of RNA binding and polymerase activity of 1b RdRp, J6CF (2a) RdRp wt and R241Q and S244D mutants, and JFH1 (2a) RdRp wt and mutant A242C/S244D suggests that steps other than RNA binding are also likely to be activated by sphingomyelin.

From a kinetic analysis of sphingomyelin activation (Fig. 1C and D), 20 sphingomyelin molecules are estimated to interact with the SBD of RdRp and activate it because sphingomyelin activation plateaued at 20 sphingomyelin molecules per HCV RdRp molecule. It is not clear whether 20 sphingomyelin molecules form a micelle or a layer structure. However, the structure of sphingomyelin is important for the activation of HCV RdRp because phosphocholine did not activate the RdRp (Fig. 3D).

To confirm these biochemical findings in HCV replication, we tested the effect of SBD mutations in HCV replicon systems with the SPT inhibitor myriocin (Fig. 5) (4, 33) because NA255 was not available. The loss-of-function mutant, HCV NN (1b) NS5B(D244S), showed lower replicon activity than NN (1b) wt and more resistance to 50 nM myriocin, which did not affect the viability of cells (4, 33), than the wt. The gain-of-function mutant, H77 (1a) NS5B(A238S/Q248E), showed higher replicon activity than H77 wt and retained myriocin sensitivity because it had the sphingomyelin binding sites 241Q and 244D. At 50 nM myriocin, another gain-of-function mutant, JFH1 (2a) NS5B(A242C/S244D), was inhibited although its activity was the same as that of JFH1 (2a) wt without myriocin because the JFH1 wt replicon had high replicon activity without myriocin (Fig. 5A). The JFH1 replicon activity may be maximal in the system; therefore, the JFH1 (2a) NS5B(A242C/S244D) replicon did not show higher activity than JFH1 (2a) wt without myriocin while H77 (1a) NS5B(A238S/Q248E) showed higher replicon activity than H77 wt.

The binding and RdRp activation activity of the amino acid 244 mutants by sphingomyelin did not differ greatly from the wt *in vitro*. However, the myriocin sensitivity of JFH1 (2a) NS5B(S244D) was demonstrated clearly. That of H77 (1a) NS5B(A238S/Q248E) indicated that sphingomyelin binding was the target of myriocin inhibition, not the sphingomyelin activation of RdRp. These data confirm the importance of 241Q, 244D, and the helix structure in SBD for HCV replication in the cells.

Sphingomyelin is the major component of the lipid raft structure/DRM where the HCV genome replicates. To confirm that the SBD is the membrane binding site of HCV RdRp, we analyzed the localization of NS5B of JFH1 (2a) wt and NS5B(A242C/S244D) replicons by membrane floating assay (Fig. 6). JFH1 (2a) NS5B wt did not localize in the DRM. However, the localization of NS5B of the JFH1 (2a) NS5B(A242C/S244D) replicon shifted to the DRM from the soluble fractions. Previously, HCV NS5B was believed to localize in the DRM by its C-terminal hydrophobic sequences (21). However, our data demonstrate that the SBD is the membrane localization domain of HCV NS5B, which agrees with the myriocin sensitivity of JFH1 (2a) NS5B(A242C/S244D) replicons (Fig. 5) and the release of HCV 1b NS5B from the DRM by another SPT inhibitor, NA255 (29).

This is the first report of RNA polymerase activation by lipids. Twenty sphingomyelin molecules interact with SBD, particularly with residues 241Q and 244D of HCV (1b) RdRp, and change the conformation of the RdRp in order to recruit RNA templates. At the same time, HCV RdRp molecules may be aligned on the sphingomyelin layer formed via interactions between the hydrocarbon chains of sphingosine and fatty acids via placement of their SBD into the layer (Fig. 7C). Consistent with previous research (3, 23, 37), our findings explain why the inhibitors of the sphingolipid biosynthetic pathway influence subgenomic replicons derived from HCV genotypes 1a and 1b but not those derived from JFH1 (2a) (Fig. 5). Most HCV isolates have 241Q in NS5B, and some of them also have 244D (Fig. 7A). These sphingomyelin interactions are new targets for the treatment of HCV.

ACKNOWLEDGMENTS

We thank C. Rice and R. Bartenshlager for the HCV H77 and Con1 plasmids, respectively. We also thank F. Chisari for Huh7.5.1 and Huh7/src cells.

This work was supported by a grant-in-aid from the Chinese Academy of Sciences (O514P51131 and KSCX1-YW-10), the Chinese 973 project (2009CB522504), and the Chinese National Science and Technology Major Project (2008ZX10002-014).

REFERENCES

1. **Adams, N. J., R. W. Chamberlain, L. A. Taylor, F. Davidson, C. K. Lin, R. M. Elliott, and P. Simmonds.** 1997. Complete coding sequence of hepatitis C virus genotype 6a. Biochem. Biophys. Res. Commun. **234**:393–396.
2. **Aizaki, H., K. J. Lee, V. M. Sung, H. Ishiko, and M. M. Lai.** 2004. Characterization of the hepatitis C virus RNA replication complex associated with lipid rafts. Virology **324**:450–461.
3. **Aizaki, H., K. Morikawa, M. Fukasawa, H. Hara, Y. Inoue, H. Tani, K. Saito, M. Nishijima, K. Hanada, Y. Matsuura, M. M. Lai, T. Miyamura, T. Wakita, and T. Suzuki.** 2008. Critical role of virion-associated cholesterol and sphingolipid in hepatitis C virus infection. J. Virol. **82**:5715–5724.
4. **Amemiya, F., S. Maekawa, Y. Itakura, A. Kanayama, A. Matsui, S. Takano, T. Yamaguchi, J. Itakura, T. Kitamura, T. Inoue, M. Sakamoto, K. Yamau-**

chi, S. Okada, A. Yamashita, N. Sakamoto, M. Itoh, and N. Enomoto. 2008. Targeting lipid metabolism in the treatment of hepatitis C virus infection. J. Infect. Dis. **197:**361–370.

5. **Binder, M., D. Quinkert, O. Bochkarova, R. Klein, N. Kezmic, R. Bartenschlager, and V. Lohmann.** 2007. Identification of determinants involved in initiation of hepatitis C virus RNA synthesis by using intergenotypic replicase chimeras. J. Virol. **81:**5270–5283.
6. **Biswal, B. K., M. M. Cherney, M. Wang, L. Chan, C. G. Yannopoulos, D. Bilimoria, O. Nicolas, J. Bedard, and M. N. James.** 2005. Crystal structures of the RNA-dependent RNA polymerase genotype 2a of hepatitis C virus reveal two conformations and suggest mechanisms of inhibition by non-nucleoside inhibitors. J. Biol. Chem. **280:**18202–18210.
7. **Blight, K. J., J. A. McKeating, J. Marcotrigiano, and C. M. Rice.** 2003. Efficient replication of hepatitis C virus genotype 1a RNAs in cell culture. J. Virol. **77:**3181–3190.
8. **Chamberlain, R. W., N. J. Adams, L. A. Taylor, P. Simmonds, and R. M. Elliott.** 1997. The complete coding sequence of hepatitis C virus genotype 5a, the predominant genotype in South Africa. Biochem. Biophys. Res. Commun. **236:**44–49.
9. **Chinnaswamy, S., I. Yarbrough, S. Palaninathan, C. T. Kumar, V. Vijayaraghavan, B. Demeler, S. M. Lemon, J. C. Sacchettini, and C. C. Kao.** 2008. A locking mechanism regulates RNA synthesis and host protein interaction by the hepatitis C virus polymerase. J. Biol. Chem. **283:**20535–20546.
10. **Chou, P. Y., and G. D. Fasman.** 1974. Prediction of protein conformation. Biochemistry **13:**222–245.
11. **Fujimoto, T., H. Kogo, K. Ishiguro, K. Tauchi, and R. Nomura.** 2001. Caveolin-2 is targeted to lipid droplets, a new "membrane domain" in the cell. J. Cell Biol. **152:**1079–1085.
12. **Gottwein, J. M., T. K. Scheel, B. Callendret, Y. P. Li, H. B. Eccleston, R. E. Engle, S. Govindarajan, W. Satterfield, R. H. Purcell, C. M. Walker, and J. Bukh.** Novel infectious cDNA clones of hepatitis C virus genotype 3a (strain S52) and 4a (strain ED43): genetic analyses and *in vivo* pathogenesis studies. J. Virol. **84:**5277–5293.
13. **Hammache, D., G. Pieroni, N. Yahi, O. Delezay, N. Koch, H. Lafont, C. Tamalet, and J. Fantini.** 1998. Specific interaction of HIV-1 and HIV-2 surface envelope glycoproteins with monolayers of galactosylceramide and ganglioside GM3. J. Biol. Chem. **273:**7967–7971.
14. **Hang, J. Q., Y. Yang, S. F. Harris, V. Leveque, H. J. Whittington, S. Rajyaguru, G. Ao-Ieong, M. F. McCown, A. Wong, A. M. Giannetti, S. Le Pogam, F. Talamas, N. Cammack, I. Najera, and K. Klumpp.** 2009. Slow binding inhibition and mechanism of resistance of non-nucleoside polymerase inhibitors of hepatitis C virus. J. Biol. Chem. **284:**15517–15529.
15. **Huang, H., F. Sun, D. M. Owen, W. Li, Y. Chen, M. Gale, Jr., and J. Ye.** 2007. Hepatitis C virus production by human hepatocytes dependent on assembly and secretion of very low-density lipoproteins. Proc. Natl. Acad. Sci. U. S. A. **104:**5848–5853.
16. **Ishii, N., K. Watashi, T. Hishiki, K. Goto, D. Inoue, M. Hijikata, T. Wakita, N. Kato, and K. Shimotohno.** 2006. Diverse effects of cyclosporine on hepatitis C virus strain replication. J. Virol. **80:**4510–4520.
17. **Kashiwagi, T., K. Hara, M. Kohara, K. Kohara, J. Iwahashi, N. Hamada, H. Yoshino, and T. Toyoda.** 2002. Kinetic analysis of C-terminally truncated RNA-dependent RNA polymerase of hepatitis C virus. Biochem. Biophys. Res. Commun. **290:**1188–1194.
18. **Kato, T., T. Date, M. Miyamoto, A. Furusaka, K. Tokushige, M. Mizokami, and T. Wakita.** 2003. Efficient replication of the genotype 2a hepatitis C virus subgenomic replicon. Gastroenterology **125:**1808–1817.
19. **Kiyosawa, K., T. Sodeyama, E. Tanaka, Y. Gibo, K. Yoshizawa, Y. Nakano, S. Furuta, Y. Akahane, K. Nishioka, R. H. Purcell, et al.** 1990. Interrelationship of blood transfusion, non-A, non-B hepatitis and hepatocellular carcinoma: analysis by detection of antibody to hepatitis C virus. Hepatology **12:**671–675.
20. **Lambot, M., S. Fretier, A. Op De Beeck, B. Quatannens, S. Lestavel, V. Clavey, and J. Dubuisson.** 2002. Reconstitution of hepatitis C virus envelope glycoproteins into liposomes as a surrogate model to study virus attachment. J. Biol. Chem. **277:**20625–20630.
21. **Lemon, S., C. Walker, M. Alter, and M. Yi.** 2007. Hepatitis C virus, p. 1253–1304. *In* D. M. Knipe, P. M. Howley, D. E. Griffin, R. A. Lamb, M. A. Martin, B. Roizman, and S. E. Straus (ed.), Fields virology, 5th ed. Lippincott Williams & Wilkins, Philadelphia, PA.
22. **Mahfoud, R., N. Garmy, M. Maresca, N. Yahi, A. Puigserver, and J. Fantini.** 2002. Identification of a common sphingolipid-binding domain in Alzheimer, prion, and HIV-1 proteins. J. Biol. Chem. **277:**11292–11296.
23. **Miyake, Y., Y. Kozutsumi, S. Nakamura, T. Fujita, and T. Kawasaki.** 1995. Serine palmitoyltransferase is the primary target of a sphingosine-like immunosuppressant, ISP-1/myriocin. Biochem. Biophys. Res. Commun. **211:**396–403.
24. **Miyanari, Y., K. Atsuzawa, N. Usuda, K. Watashi, T. Hishiki, M. Zayas, R. Bartenschlager, T. Wakita, M. Hijikata, and K. Shimotohno.** 2007. The lipid droplet is an important organelle for hepatitis C virus production. Nat. Cell Biol. **9:**1089–1097.
25. **Murayama, A., T. Date, K. Morikawa, D. Akazawa, M. Miyamoto, M. Kaga, K. Ishii, T. Suzuki, T. Kato, M. Mizokami, and T. Wakita.** 2007. The NS3 helicase and NS5B-to-3′X regions are important for efficient hepatitis C virus strain JFH-1 replication in Huh7 cells. J. Virol. **81:**8030–8040.
26. **Murayama, A., L. Weng, T. Date, D. Akazawa, X. Tian, T. Suzuki, T. Kato, Y. Tanaka, M. Mizokami, T. Wakita, and T. Toyoda.** 2010. RNA polymerase activity and specific RNA structure are required for efficient HCV replication in cultured cells. PLoS Pathog. **6:**e1000885.
27. **Ostermeyer, A. G., J. M. Paci, Y. Zeng, D. M. Lublin, S. Munro, and D. A. Brown.** 2001. Accumulation of caveolin in the endoplasmic reticulum redirects the protein to lipid storage droplets. J. Cell Biol. **152:**1071–1078.
28. **Saito, I., T. Miyamura, A. Ohbayashi, H. Harada, T. Katayama, S. Kikuchi, Y. Watanabe, S. Koi, M. Onji, Y. Ohta, et al.** 1990. Hepatitis C virus infection is associated with the development of hepatocellular carcinoma. Proc. Natl. Acad. Sci. U. S. A. **87:**6547–6549.
29. **Sakamoto, H., K. Okamoto, M. Aoki, H. Kato, A. Katsume, A. Ohta, T. Tsukuda, N. Shimma, Y. Aoki, M. Arisawa, M. Kohara, and M. Sudoh.** 2005. Host sphingolipid biosynthesis as a target for hepatitis C virus therapy. Nat. Chem. Biol. **1:**333–337.
30. **Shi, S. T., K. J. Lee, H. Aizaki, S. B. Hwang, and M. M. Lai.** 2003. Hepatitis C virus RNA replication occurs on a detergent-resistant membrane that cofractionates with caveolin-2. J. Virol. **77:**4160–4168.
31. **Simister, P., M. Schmitt, M. Geitmann, O. Wicht, U. H. Danielson, R. Klein, S. Bressanelli, and V. Lohmann.** 2009. Structural and functional analysis of hepatitis C virus strain JFH1 polymerase. J. Virol. **83:**11926–11939.
32. **Tsukiyama-Kohara, K., S. Tone, I. Maruyama, K. Inoue, A. Katsume, H. Nuriya, H. Ohmori, J. Ohkawa, K. Taira, Y. Hoshikawa, F. Shibasaki, M. Reth, Y. Minatogawa, and M. Kohara.** 2004. Activation of the CKI-CDK-Rb-E2F pathway in full genome hepatitis C virus-expressing cells. J. Biol. Chem. **279:**14531–14541.
33. **Umehara, T., M. Sudoh, F. Yasui, C. Matsuda, Y. Hayashi, K. Chayama, and M. Kohara.** 2006. Serine palmitoyltransferase inhibitor suppresses HCV replication in a mouse model. Biochem. Biophys. Res. Commun. **346:**67–73.
34. **Wasley, A., and M. J. Alter.** 2000. Epidemiology of hepatitis C: geographic differences and temporal trends. Semin. Liver Dis. **20:**1–16.
35. **Watashi, K., N. Ishii, M. Hijikata, D. Inoue, T. Murata, Y. Miyanari, and K. Shimotohno.** 2005. Cyclophilin B is a functional regulator of hepatitis C virus RNA polymerase. Mol. Cell **19:**111–122.
36. **Weng, L., J. Du, J. Zhou, J. Ding, T. Wakita, M. Kohara, and T. Toyoda.** 2009. Modification of hepatitis C virus 1b RNA polymerase to make a highly active JFH1-type polymerase by mutation of the thumb domain. Arch. Virol. **154:**765–773.
37. **Yasuda, S., H. Kitagawa, M. Ueno, H. Ishitani, M. Fukasawa, M. Nishijima, S. Kobayashi, and K. Hanada.** 2001. A novel inhibitor of ceramide trafficking from the endoplasmic reticulum to the site of sphingomyelin synthesis. J. Biol. Chem. **276:**43994–44002.
38. **Zhong, J., P. Gastaminza, G. Cheng, S. Kapadia, T. Kato, D. R. Burton, S. F. Wieland, S. L. Uprichard, T. Wakita, and F. V. Chisari.** 2005. Robust hepatitis C virus infection in vitro. Proc. Natl. Acad. Sci. U. S. A. **102:**9294–9299.

Journal of Medical Virology 82:1364–1370 (2010)

Secondary Structure of the Amino-Terminal Region of HCV NS3 and Virological Response to Pegylated Interferon Plus Ribavirin Therapy for Chronic Hepatitis C

Mai Sanjo,[1] Takafumi Saito,[1]* Rika Ishii,[1] Yuko Nishise,[1] Hiroaki Haga,[1] Kazuo Okumoto,[1] Junitsu Ito,[1] Hisayoshi Watanabe,[1] Koji Saito,[1] Hitoshi Togashi,[2] Kazuto Fukuda,[3] Yasuharu Imai,[3] Ahmed El-Shamy,[4] Lin Deng,[4] Ikuo Shoji,[4] Hak Hotta,[4] and Sumio Kawata[1]

[1]*Department of Gastroenterology, Yamagata University School of Medicine, Yamagata, Japan*
[2]*Health Administrative Center, Yamagata University, Yamagata, Japan*
[3]*Division of Gastroenterology, Ikeda Municipal Hospital, Osaka, Japan*
[4]*Division of Microbiology, Kobe University Graduate School of Medicine, Kobe, Japan*

The aim of the study was to identify a predictive marker for the virological response in hepatitis C virus 1b (HCV-1b)-infected patients treated with pegylated interferon plus ribavirin therapy. A total of 139 patients with chronic hepatitis C who received therapy for 48 weeks were enrolled. The secondary structure of the 120 residues of the amino-terminal HCV-1b non-structural region 3 (NS3) deduced from the amino acid sequence was classified into two major groups: A and B. The association between HCV NS3 protein polymorphism and virological response was analyzed in patients infected with group A ($n = 28$) and B ($n = 40$) isolates who had good adherence to both pegylated interferon and ribavirin administration (>95% of the scheduled dosage) for 48 weeks. A sustained virological response (SVR) representing successful HCV eradication occurred in 33 (49%) in the 68 patients. Of the 28 patients infected with the group A isolate, 18 (64%) were SVR, whereas of the 40 patients infected with the group B isolate only 15 (38%) were SVR. The proportion of virological responses differed significantly between the two groups ($P < 0.05$). These results suggest that polymorphism in the secondary structure of the HCV-1b NS3 amino-terminal region influences the virological response to pegylated interferon plus ribavirin therapy, and that virus grouping based on this polymorphism can contribute to prediction of the outcome of this therapy. ***J. Med. Virol. 82:1364–1370, 2010.*** © 2010 Wiley-Liss, Inc.

KEY WORDS: hepatitis C; interferon; ribavirin; interaction; polymorphism

INTRODUCTION

Hepatitis C virus (HCV) is the major pathogen that causes chronic liver diseases with a risk of progression to cirrhosis and hepatocellular carcinoma. Currently, the standard treatment for chronic hepatitis C is antiviral therapy using pegylated interferon (Peg-IFN) plus ribavirin (RBV), and this approach is most effective for eradication of HCV viremia. However, even with the widely used treatment regimen of 48 weeks, the rate of sustained virological response (SVR), which indicates eradication of viremia, is still approximately 50% for patients infected with the therapy-resistant HCV genotype 1b (HCV-1b) with a high viral load [Manns et al., 2001; Bruno et al., 2004; Hadziyannis et al., 2004]. It would be useful to predict the virological response to this therapy and to identify patients who would obtain beneficial therapeutic effects before treatment, in order to avoid any serious side effect and to eliminate those who would not be helped by the treatment. In the future it will be important to establish a protocol of tailor-made medicine for chronic hepatitis C.

Grant sponsor: Grant-in-Aid for Scientific Research; Grant number: 21590824; Grant sponsor: Global Center of Excellence program of the Japan Society for the Promotion of Science (Yamagata University School of Medicine and Kobe University Graduate School of Medicine); Grant sponsor: Ministry of Health, Labor and Welfare of Japan.

*Correspondence to: Takafumi Saito, M. D., Department of Gastroenterology, Yamagata University School of Medicine, 2-2-2 Iida-nishi, Yamagata 990-9585, Japan.
E-mail: tasaitoh@med.id.yamagata-u.ac.jp

Accepted 6 March 2010
DOI 10.1002/jmv.21818
Published online in Wiley InterScience (www.interscience.wiley.com)

Both the HCV genotype and pre-treatment viral load are major viral factors that influence the response to IFN-based antiviral therapy, but IFN resistance is also partly due to variation of the amino acid sequence encoded by HCV itself. Enomoto et al. [1996] proposed that variation of 40 amino acids within the NS5A region (aa 2,209–2,248), which is referred to as the IFN sensitivity-determining region (ISDR), is well correlated with IFN responsiveness. ISDR and its adjacent sequence bind and inhibit the enzymatic activity of a double-stranded RNA-activated protein kinase (PKR), which can have an antiviral effect, and therefore the combined region is referred to as the PKR-binding domain (PKR-BD) [Gale et al., 1997, 1998]. A correlation between sequence variation in the PKR-BD and IFN responsiveness has been reported [Nousbaum et al., 2000], and some reports show a correlation between IFN responsiveness and the sequence diversity of variable region 3 (V3) (aa 2,356–2,379) or surrounding regions near the carboxy terminus of NS5A [Murphy et al., 2002; Sarrazin et al., 2002; Puig-Basagoiti et al., 2005]. A high degree of amino acid substitution in the V3 and pre-V3 regions (aa 2,334–2,355) of NS5A, which is referred to as the IFN/RBV resistance-determining region (IRRDR) (aa 2,334–2,379), has been associated with SVR in Peg-IFN/RBV combination therapy for patients infected with HCV-1b [El-Shamy et al., 2007, 2008]. In addition to these findings in non-structural proteins of the virus, amino acid substitution in a structural region of HCV has been reported to be a predictive viral marker for the virological response to PegIFN/RBV therapy. Amino acid polymorphisms in the HCV core region (Arg70 vs. Gln70 and Leu91 vs. Met91) correlate with virological outcome and on-treatment viral kinetics in Peg-IFN/RBV therapy [Akuta et al., 2006, 2007], and a double wild-type HCV core (Arg70 and Leu91) may be a significant predictor of SVR in Peg-IFN/RBV therapy [Akuta et al., 2007].

Interactions between viral and host proteins in infected cells may influence therapeutic effects and the natural history of infection, since the HCV NS3 region has a significant effect on immunity. The amino-terminal part of this region encodes a serine protease, for which the minimum activity has been mapped to a region between aa 1,059 and 1,204 [Yamada et al., 1998]. The serine protease inactivates Cardif, a caspase recruitment domain (CARD)-containing adaptor protein that interacts with the RNA helicase retinoic acid inducible gene 1 (RIG-1)-dependent antiviral pathway in infected cells [Foy et al., 2003; Meylan et al., 2005; Evans and Seeger, 2006]. This action inhibits phosphorylation and subsequent heterodimerization of interferon regulatory factor-3 (IRF-3), which is essential for activation of IFN signaling through translocation of IRF-3 heterodimers into the nucleus, and eventually blocks IFN-beta production. In addition, inactivation of IRF-3 is postulated to influence the therapeutic effect of IFN-based antiviral therapy, because the IRF-3 heterodimer translocates into the nucleus to bind to the IFN-stimulated response element that produces many antiviral proteins, including 2′,5′-oligoadenylate synthetase and PKR [Nakaya et al., 2001; Grandvaux et al., 2002]. Collectively, these findings suggest that polymorphisms in HCV NS3 structure deduced from sequence variation may influence IFN-related signaling and the antiviral effect of IFN-based anti-HCV therapy.

We have focused on polymorphisms in the secondary structure of the viral polyprotein that interacts with host proteins involved in immunity, with the aim of identification of predictive viral markers for the response to Peg-IFN/RBV therapy. In this study, we examined the potential correlation between polymorphisms in the secondary structure of the HCV NS3 amino-terminal region and virological responses to Peg-IFN/RBV therapy in patients infected with HCV-1b with a high viral load.

PATIENTS AND METHODS

Patients and Treatment Regimen With Peg-IFN Plus Ribavirin

A total of 139 consecutive patients diagnosed with chronic hepatitis C were enrolled in the study from December 2004 to March 2007. These patients included 81 men and 58 women, and were aged from 31 to 75 years old (mean ± SD, 56.8 ± 8.7 years old). All patients were infected with HCV-1b with a high viral load of over 100 KIU/ml, and all received Peg-IFN/RBV therapy. Patients with alcoholic liver injury, autoimmune liver disease, and those who had symptoms of decompensated cirrhosis including ascites were excluded. Briefly, all patients were treated with a combination of Peg-IFN-alpha 2b (Pegintron®; Schering-Plough, Kenilworth, NJ) and RBV (Rebetol®; Schering-Plough) for 48 weeks. Peg-IFN was administered subcutaneously once a week and RBV was given orally twice a day for the total dose. The dosages were determined on the basis of body weight according to the Japanese standard prescription information supplied by the Japanese Ministry of Health, Labour and Welfare, and there was a limit for calculating the optimized dose: patients with body weights of 35–45, 46–60, 61–75, and 76–90 kg were given Peg-IFN at doses of 60, 80, 100, and 120 μg, respectively, and those with body weights of <60, 60–80, and >80 kg were given RBV at doses of 600, 800, and 1,000 mg, respectively. The dose of Peg-IFN or RBV was reduced according to the Japanese standard criteria based on the white blood cell count, neutrophil count, hemoglobin concentration and platelet count [Hiramatsu et al., 2008].

Virological Tests and Response to Peg-IFN Plus Ribavirin

Virological responses were evaluated at 12 weeks after the start of treatment with an early depletion of viremia referred to as an early virological response (EVR), at the end of treatment with depletion of viremia referred to as an end of treatment virological response (ETR), and at 24 weeks after completion of treatment,

with a clinical outcome of a sustained virological response (SVR) representing successful HCV eradication. All patients were negative for hepatitis B surface antigen. Quantification of serum HCV RNA was performed using an RT-PCR-based commercial kit (Amplicor HCV monitor test, ver. 2.0, Roche Diagnostics, Tokyo, Japan). This Amplicor HCV RNA assay has a lower limit of detection of 50 IU/ml. SVR was determined by monitering negativity for HCV RNA monthly for 6 months. The real-time PCR assay kit (COBAS TaqMan HCV Auto, Roche Diagnostics) for more precise quantitation of HCV viremia has recently become available and pre-treatment viral titers were re-evaluated using preserved serum samples. This real-time PCR assay has a lower limit of detection of 15 IU/ml. The study protocol was approved by the Ethics Committee of Yamagata University Hospital. Informed consent was obtained from all patients.

PCR Amplification of the Amino-Terminal Region of NS3

RNA was extracted from 50 µl of serum using an RNeasy Mini kit (Qiagen, Tokyo, Japan). To amplify the region of the HCV genome encoding the amino-terminal region of NS3 (1,027–1,206), a one-step PCR was performed in a tube using the Superscript One-Step RT-PCR kit with Platinum Taq (Gibco-BRL, Tokyo, Japan) and an outer set of primers: NS3-F1 (sense primer; 5′-ACA CCG CGG CGT GTG GGG ACA T-3′; nucleotides 3,295–3,316) and NS3-AS2 (antisense primer; 5′-GCT CTT GCC GCT GCC AGT GGG A-3′; nucleotides 4,040–4,019), as reported previously [Ogata et al., 2002a, 2003]. PCR was initially performed at 45°C for 30 min at RT and then at 94°C for 2 min, followed by the first-round PCR for forty 3-min cycles at 94°, 55°, and 72°C for 1 min each. The second-round PCR was performed with *Pfu* DNA polymerase (Promega, Tokyo, Japan) and an inner set of primers: NS3-F3 (sense primer; 5′-CAG GGG TGG CGG CTC CTT-3′; nucleotides 3,390–3,407) and NS3-AS1 (antisense primer; 5′-GCC ACT TGG AAT GTT TGC GGT A-3′; nucleotides 4,006–3,985). The second-round PCR was performed for 35 cycles, with each cycle consisting of 1 min at 94°C, 1.5 min at 55°C, and 3 min at 72°C. This method allowed amplification of the corresponding portion of the HCV genome from HCV-1b RNA-positive samples. The amplified fragments were purified with a QIAquick PCR purification kit (Qiagen) and directly sequenced (without being subcloned) in both directions using a dRhodamine Terminator Cycle Sequencing Ready Reaction kit and an ABI 377 sequencer (Applied Biosystems, Tokyo, Japan).

Classification of the Secondary Structure of the HCV-1b NS3 Amino-Terminal Region

The secondary structure of the amino-terminal region of HCV NS3 was predicted by computer-assisted Robson analysis [Garnier et al., 1978] with Genetyx-Mac software (ver.10.1; Software Development Co., Tokyo, Japan). Previously, the full-length secondary structure of the HCV-1b NS3 region was analyzed, and this showed that the secondary structure deduced from the carboxy-terminal 60 residues was well conserved in terms of linear structure, without any turn structure [Ogata et al., 2002a]. We have shown that the secondary structure of the 120 residues in the amino-terminal region of HCV-1b NS3 can be classified into two major groups: A and B (Fig. 1) [Ogata et al., 2002a, 2003]. Briefly, the criteria for this classification are as follows: in group A isolates, the carboxy-terminal 20 residues (aa 1,125–1,146) are oriented leftward relative to a domain composed of the remaining amino-terminal region; whereas in group B isolates, the same 20 residues are oriented rightward relative to the rest of the amino-terminal domain.

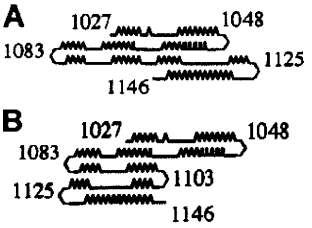

Fig. 1. Secondary structure of the 120 amino-terminal residues of HCV-1b nonstructural 3 (NS3) region classified into two major groups: A and B. The looped, zigzag, straight, and bent lines represent α-helix, β-sheet, coil, and turn structures, respectively. The numbers indicate amino acid positions. **A**: Group A, (**B**) Group B.

Analysis of Amino Acid Substitutions in the Core Region

To amplify a region of the HCV genome encoding the core region including positions 70 and 91, reverse transcription and the first-round PCR were performed in a tube by the Superscript One-Step RT-PCR kit with Platinum *Taq* (Gibco-BRL) and an outer set of primers, followed by second-round PCR with an inner set of primers in accordance with procedures reported previously [Ogata et al., 2002b]. The sequences of the amplified fragments were determined by direct sequencing.

Statistical Analysis

Data were analyzed by a χ^2 test for independence with a two-by-two contingency table and a Student t-test. A P-value <0.05 was considered significant.

RESULTS

Virological Response *and Adherence* to the Peg-IFN Plus Ribavirin Regimen

Rates of virological responses in patients treated with PegIFN/RBV combination therapy for 48 weeks are shown in Figure 2. Of the 139 patients enrolled in the study, SVR, non-SVR and cessation of therapy occurred in 58 (42%), 62 (45%), and 19 (14%), respectively. Serious